Germanium-Based Batteries

International Edition: DOI: 10.1002/anie.201509651
German Edition: DOI: 10.1002/ange.201509651

Germanium-Based Nanomaterials for Rechargeable Batteries

Songping Wu, Cuiping Han, James Iocozzia, Mingjia Lu, Rongyun Ge, Rui Xu, and Zhiqun Lin**

Keywords:
conducting materials · electrochemistry · energy conversion · germanium · rechargeable batteries

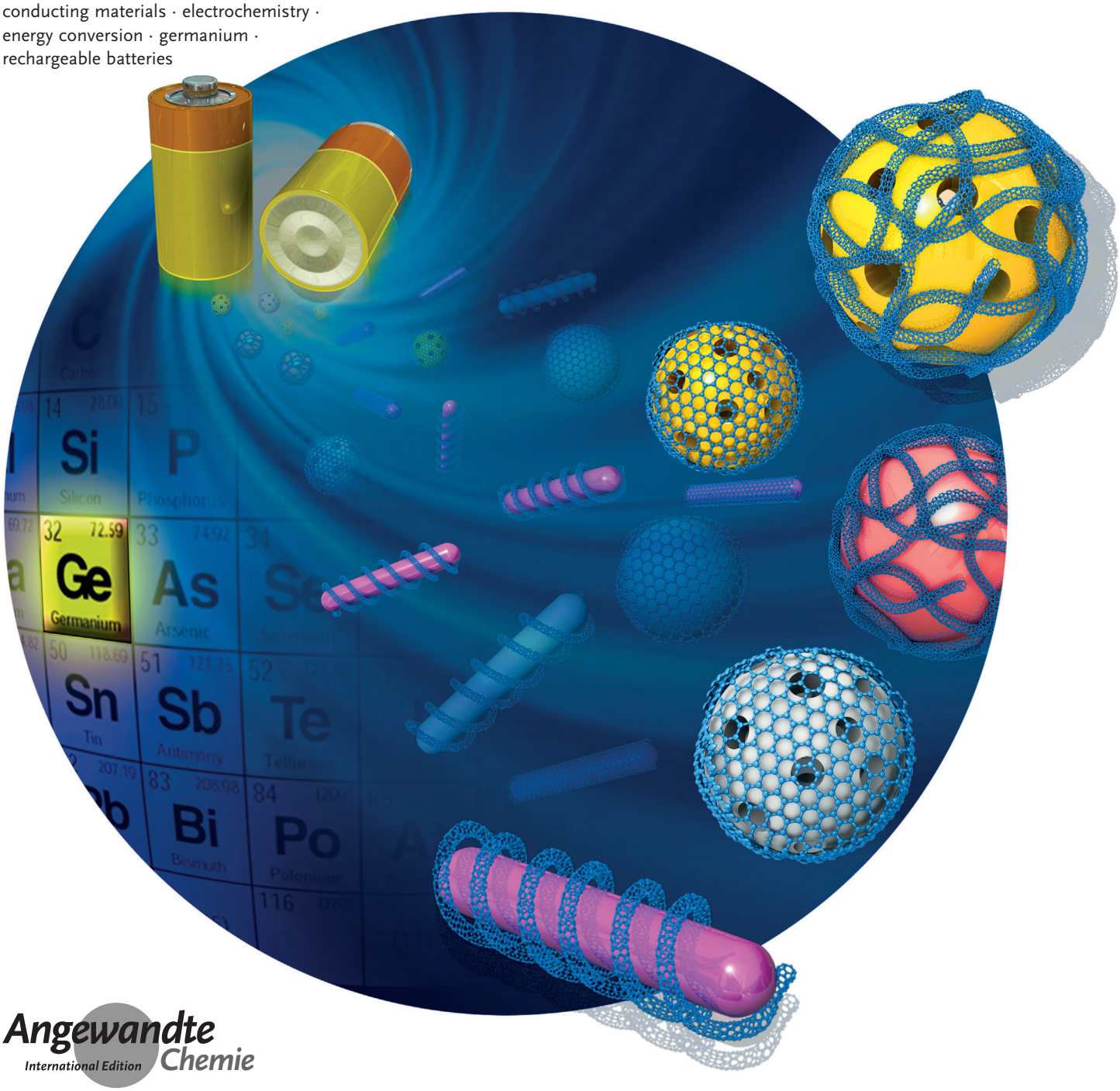

Germanium-based nanomaterials have emerged as important candidates for next-generation energy-storage devices owing to their unique chemical and physical properties. In this Review, we provide a review of the current state-of-the-art in germanium-based materials design, synthesis, processing, and application in battery technology. The most recent advances in the area of Ge-based nanocomposite electrode materials and electrolytes for solid-state batteries are summarized. The limitations of Ge-based materials for energy-storage applications are discussed, and potential research directions are also presented with an emphasis on commercial products and theoretical investigations.

From the Contents

1. Introduction

Today, new commercially viable electronic devices are emerging from small-scale benchtop laboratory curiosities at an impressive rate. Cleaner and longer-lasting energy-storage devices are of the utmost importance in all current and future technologies. As a result, several new battery concepts have been developed including flow batteries,[1,2] Li–S and sodium-ion batteries, Li–O_2 batteries,[3,4] thermal batteries,[5] sodium–sulfur batteries,[6] sodium breathing batteries (Na_2O),[7] magnesium-ion batteries,[8] and many more. The requirements for next-generation batteries are particularly demanding and include larger capacity, improved safety, faster recharge, and lower cost. For various devices, meeting all of these requirements presents a standing challenge preventing the jump to industrial development. A more incremental target for next-generation batteries may be more realistic. For example, a single-battery cost of 0.15$ Wh^{-1}, with an energy density of more than 180 $Wh\,Kg^{-1}$ at 270 $W\,Kg^{-1}$ after 1000 cycles is a reasonable incremental benchmark for assessing new technologies.[4a,9]

Fortunately, the diverse and voluminous research in next-generation energy-storage technologies is capable of succeeding in developing better energy-storage devices for satisfying many immediate needs. Among the current candidates, lithium-ion batteries (LIBs) represent the state-of-the-art technology in rechargeable energy-storage devices and currently occupy the largest portion of the marketplace for meeting an increasingly diverse range of applications. By no means a new technology, LIBs have been the dominant mobile energy provider in peoples' lives for more than 20 years.[10] However, the presence of high-energy devices, such as electrical vehicles, stationary electrical storage, smart grids, and even portable and wearable electronic devices has placed higher requirements on current LIB technologies. In particular, electrical vehicles are becoming far more ubiquitous because of the remarkable increase in energy efficiency. Therefore, rechargeable ultra-high-energy-storage devices have attracted great attention and the desire to improve even further.[10]

In 2012, the JCESR (Joint Center for Energy Storage Research) stated a very aggressive goal for the commercial battery packs used in electric vehicles of 400 $Wh\,kg^{-1}$ by 2017.[11] Such a goal is too large to achieve for conventional batteries. Current LIBs afford an energy density of 120 $Wh\,kg^{-1}$ [12,13] which is expected to reach 180–200 $Wh\,kg^{-1}$ in the near future (ca. 2–3 years). While this is encouraging, the theoretical capacity of commercial anode materials (i.e., graphite) is only 372 $mA\,h\,g^{-1}$ which severely limits the improvement of overall energy-storage performance.[14] The need for high-power applications have called for the development of high-performance electrode materials because they have been a major limiting factor in overall rechargeable battery performance. Recently, significant effort has focused on alternatives (i.e., transition-metal oxides and metals, such as Si, Sn) for electrode construction to explore potentially low-cost, high-performance materials for replacement of current electrode materials.[13,15–17]

As typical new-concept battery materials, oxides (including ternary oxides[18,19]), sulfides,[20–22] and metals[23–25] have been extensively investigated due to their distinctive advantages including low cost, their abundance and high storage capacity as electrodes in LIBs and sodium ion batteries (SIBs).[26,27] Among candidate materials, metals are believed to deliver the highest Li-storage capability owing to simple elemental addition.[28,29] Recently, silicon-based materials have also gained prominence as potential next-generation anode materials with investigations underway by several companies.[30,31] For example, pilot-plant-synthesized Si/C and SiO_x/C materials can achieve reversible capacities of 450 $mA\,h\,g^{-1}$ at 180 $mA\,g^{-1}$ after 800 cycles, and 700 $mA\,hg^{-1}$ at 180 $mA\,g^{-1}$ after 400 cycles. Unfortunately, low conductivity and large volume expansion (> 300 %) during lithiation and deliathiation still remain the biggest obstacles for the commercialization of silicon-based anodes in LIBs.[32] Herein, the focus will be on the metal germanium and its applications in energy-storage research. This material has an increasing prominence as an anode material due to its high

[*] Prof. S. Wu, M. Lu, R. Ge, R. Xu
School of Chemistry and Chemical Engineering
South China University of Technology
Guangzhou city, Guangdong province, 510641 (China)
E-mail: chwsp@scut.edu.cn
Dr. C. Han, J. Iocozzia, Prof. Z. Lin
School of Materials Science and Engineering, Georgia Institute of Technology
Atlanta, Georgia 30332 (USA)
E-mail: zhiqun.lin@mse.gatech.edu

theoretical capacity (1600 mA h g^{-1} for $Li_{4.4}Ge$), excellent electrical conductivity (ca. 100 times higher than Si), rapid Li^+ mobility (400 times faster than in Si) and remarkable mechanical strength.

Germanium is a hard grayish-white metalloid with an attractive metallic luster. In the process of magma crystallization, germanium can replace silicon or aluminum in mineral lattices, and unevenly scatter in silicate rocks. In 1886, Winkler isolated a new element from argyrodite, and subsequently named it germanium in honor of his homeland. Germanium is sparsely distributed around the earth. In nature, it mostly exists in a mineral form of various types at low concentration. Consequently, it has been difficult to produce or find sufficient mineral concentrations to warrant major industrial utilization.

As a result, the industrial applications of germanium were ignored for many years after its discovery until germanium made its debut in the semiconductor industry in the mid-1940s. In fact, germanium was first established as the lead material in the early stages of the development of semiconductor electronics before it was substituted for a more inexpensive and abundant material: silicon. However, the unique advantages associated with germanium, such as a high electronic mobility (band gap of Ge: 0.66 eV at 300 K), high frequency (for Ge-based devices) and remarkable mechanical strength have afforded applications in the fields of high frequency,[33] far-infrared, and aerospace electronics. Today, fiber-optic, infrared optics, photoluminescence,[34,35] solar cells,[36] hydrogen-storage alloys,[37] superconductors,[38] and catalysts have increasingly utilized germanium (Scheme 1).[39] In 2011, about 118 tones of germanium were manufactured worldwide, mostly in China (80 t), Russia (5 t), and the United States (3 t). It is clear that the relevance of germanium-based technologies, far from being obsolete, is burgeoning despite the difficulties of its acquisition.

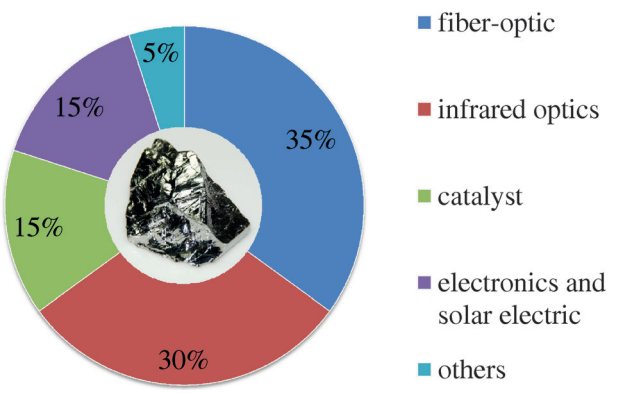

Scheme 1. Breakdown of industrial germanium consumption by sector (2007). Inset: a polycrystalline block of germanium with unevenly cleaved surfaces.

This Review will focus on current applications and future development of germanium in next-generation battery technology. There are several recent Reviews on metal-based materials for energy-storage and conversion[40–43] focusing on the synthesis of Ge nanowires,[44] primarily via the colloidal route.[45] However, a critical Review that focuses exclusively on germanium-based materials for applications in next-generation batteries has not been reported. This Review aims to provide an up-to-date and comprehensive summary of recent advances in the rational design of germanium-based composites with a focus on anodes and solid electrolytes for

Dr. Songping Wu obtained his Ph.D. (2002) with Prof. Guobang Gu at South China University of Technology, China. Since 2004 he has been an associate professor at South China University of Technology. He was also a visiting scholar at The Hong Kong Polytechnic University (2006–2007) and Georgia Institute of Technology (2013–2014). He works on advanced functional ceramic materials and Li-ion battery materials. His current research interests are focused on graphene-based materials for lithium-ion batteries.

James Iocozzia is a graduate student in the School of Materials Science and Engineering at the Georgia Institute of Technology. He received his B.S. in Polymer and Fiber Engineering from the Georgia Institute of Technology in 2012. His research interests include nanocomposites, block copolymers and hyperbranched polymer systems for the development of functional hard and soft organic/inorganic nanomaterials. He is a National Defense Science and Engineering Graduate (NDSEG) Fellow, a Graduate Student Presidential Fellow, an NSF EAPSI Fellow, and a BIONIC Scholar.

Cuiping Han received her B.S. degree from China University of Petroleum (Huadong) in 2010 and Ph.D. degree from Tsinghua University in 2015 with Prof. Baohua Li. She visited Georgia Institute of Technology during 2014–2015 as a visiting scholar in the group of Prof. Zhiqun Lin. She is now a joint postdoc (Xiangjiang scholar program) of Tsinghua University and Chinese University of Hong Kong with Prof. Ching-Ping Wong. Her research is focused on lithium-ion batteries and supercapacitors.

Mingjia Lu received her Bachelor's degree from the Institute of Physical Chemistry, Henan Polytechnic University (China) in 2012. She is currently pursuing her Master's degree at the School of Chemistry and Chemical Engineering, South China University of Technology with Prof Songping Wu. Her current research interests focus on the elevated-temperature performance of graphene-based anode materials for advanced Li-ion batteries.

next-generation storage energy devices (LIBs and SIBs). It should be noted that Ge-based materials can also be utilized as cathode materials, but such efforts lie outside the scope of this Review.[46] Details regarding established and generalizable synthetic routes, structural configurations spanning several dimensions, electrochemical performances, and Li-cycling mechanisms are also addressed (Scheme 2).

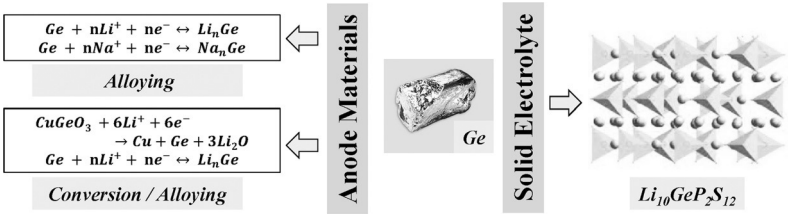

Scheme 2. Left: the typical electrochemical reaction mechanism for lithiation via alloying and conversion. Right: representative structure of a solid-electrolyte compound.

2. Anode Materials for LIBs

As proposed by Reddy et al.,[47] elements such as Si, Sb, Sn, In, Cd, and Mg,[48] can facilitate lithium storage and cycling behavior via alloying–dealloying reactions at potentials less than 1 V versus Li metal. Therefore, such elements are prospective anode materials for LIBs. The general Li-cycling mechanism of metal alloying/dealloying in LIBs is given by Equation (1).

$$\text{Alloying reaction}: \quad \mathrm{M} + n\mathrm{Li}^+ + ne^- \rightleftharpoons \mathrm{Li}_n\mathrm{M} \qquad (1)$$

However, repeated investigations have demonstrated the unreliable Li-cycle stability of Sn, Si, Sb, etc. via alloying–dealloying reactions due to large volume changes during Li-cycling. In some cases the changes can be as high as 434% for silicon, 382% for germanium, and 305% for tin.[49] This inevitably leads to "electrochemical pulverization" of the active material on the electrode. Ultimately, this leads to electrode disintegration and capacity fading under long-term cycling.

2.1. Background

2.1.1. Synthesis of germanium nanostructures

It is generally accepted that the proper processing and synthetic routes can lead to unique metal morphologies, sizes, and spatial arrangements. Consequently, distinct structure–property relationships can be established with each having potential applications in different areas. To obtain novel structured Ge nanomaterials with improved electrochemical performance, several approaches have been investigated, including but not limited to the following examples: electrodeposition of Ge nanowires,[50] microfabrication of Ge microbars,[51] Vapor-liquid-solid (VLS) growth[52] of single crystalline Ge nanowires, molten salt synthesis of Ge nanoparticles,[53] gas-phase photolysis,[54] radio frequency sputtering synthesis of Ge nanofilms,[55] chemical vapor deposition (CVD)[56] of porous Ge walls, and electrodeposition from ionic liquid to produce Ge nanotubes (Figure 1).[57] Notably, ion-beam modification is of great use in forming "nanostructured" germanium (known as "voided", "porous", "nanoporous", "cratered", and "honeycomb" Ge).[40] These designed structures afford at least one of the following benefits:

1) a sufficient number of voids to accommodate volume changes during cycling;
2) fast transport pathways for electrons and lithium ions;
3) stable in situ formed SEI layers.[41]

The following Sections will elaborate on these benefits where they appear as well as other useful and interesting structure-property relationships.

Rongyun Ge completed her bachelor studies at Henan University of Technology (China) in 2012. She is currently pursuing her Master's degree at South China University of Technology with Prof. Songping Wu.

Rui Xu received her Bachelor's degree from the Institute of Chemical and Materials Engineering at Hubei Polytechnic University (China) in 2012. She is currently pursuing her Master's degree at the School of Chemistry and Chemical Engineering, South China University of Technology with Prof. Songping Wu. Her current research interests are focused on graphene-based anode materials for lithium-ion batteries.

Zhiqun Lin is a Professor in the School of Materials Science and Engineering at the Georgia Institute of Technology. He received his Ph.D. in Polymer Science and Engineering from the University of Massachusetts, Amherst in 2002 with Prof. Tom Russell. His research interests include lithium-ion batteries, perovskite solar cells, polymer solar cells, dye-sensitized solar cells, semiconductor organic–inorganic nanocomposites, photocatalysis, hydrogen generation, quantum dots (rods), polymers, hierarchical structure formation and interfacial properties.

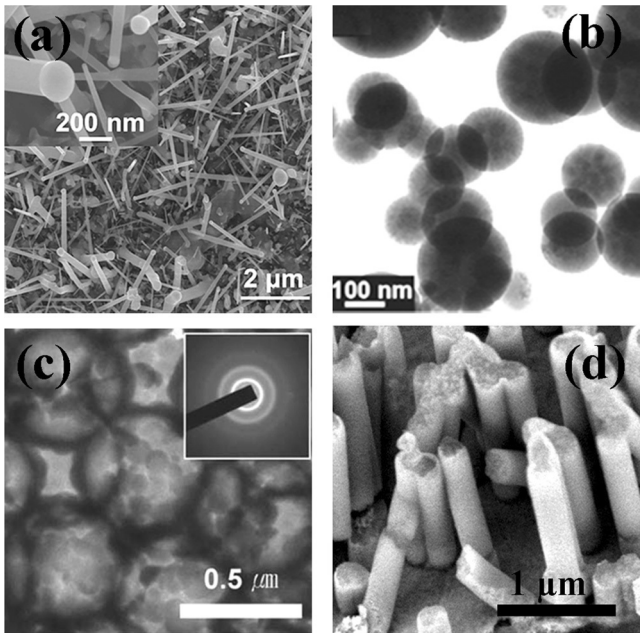

Figure 1. Typical micro- and nanostructures by different routes: a) Plan-view SEM image of as-synthesized Ge nanowires via VLS growth. Reproduced with permission from Ref. [52] Copyright 2014 The Royal Society of Chemistry. b) TEM images of Ge NCs synthesized via gas-phase photolysis. Reproduced with permission from Ref. [54] Copyright 2012 The American Chemical Society. c) High-magnification TEM image of Ge inverse opals with porous walls prepared via CVD. Inset: the selected-area electron diffraction (SAED) pattern. Reproduced with permission from Ref. [56] Copyright 2012 The Royal Society of Chemistry. d) Cross-sectional view of Ge nanotubes produced via electrodeposition. Reproduced with permission from Ref. [57] Copyright 2014 Elsevier.

2.1.2. *Li-Storage Mechanism*

Regarding metallic Ge for LIB anode materials, extensive fundamental research has been performed and significant understanding has been obtained to date. Among the many benefits of Ge that warrant its active role in LIBs, the decrease in diffusion barriers,[58] large hole concentration of 8×10^{19} cm^{-3}, and low resistivity of 4×10^{-5} $\Omega\,cm^{-1}$ in several morphologies are particularly attractive.[59]

2.1.2.1. *Li Mobility in Li–Ge Alloys*

Early research on lithium insertion found that the initial crystalline Ge underwent a two-step phase transformation process. First it forms an intermediate amorphous Li_xGe before assuming the regular crystalline $Li_{15}Ge_4$ phase. Porous nanowires exhibited fast lithiation/delithiation rates and excellent mechanical strength.[60] Intriguingly, alloying between Li and a metal is energetically favorable for Li–Ge alloys. Therefore, Li interstitials can easily migrate in the host material.[49] Furthermore, Li transport efficiency in Ge electrodes remains unchanged during both charging and discharging.[30] First-principle density functional theory (DFT) showed a lack of orientational dependence in lithiation onset voltages in Ge.[61] Recently,[62] it was found that the Li–Ge interaction tends to dictate the Li mobility in crystalline Ge (c-Ge) electrodes ($D_{Li}=10^{-11}$ cm^2s^{-1}). The mobility subsequently increases to around 10^{-7} cm^2s^{-1} as lithiation continues. This shows that rapid Li diffusion in amorphous Li_xGe is directly related to the atomic rearrangements of the host Ge atoms even at the very early stages of lithiation.

2.1.2.2. *Li-Storage and Structural Stability in Li–Ge Alloys*

Recently, to highlight the Li-storage mechanism in Ge-based materials during cycling, much effort has been devoted to investigate the lithiation/delithiation process of Ge anode materials. In general, the formation of amorphous of Li–Ge alloys plays a vital role in providing good Li-storage capability during the discharge/charge process.[63–65] The conversion between crystalline and amorphous Ge was believed to occur via a simple amorphous-to-crystalline interconversion between Li_9Ge_4[63] and $Li_{15}Ge_4$[66] during Li-cycling. Zeilinger and Fässler subsequently investigated more Li–Ge alloys to better understand the underlying mechanisms in Ge-based electrodes.[64] For example, it was found that locally formed, lithium-rich sections of the Li–Ge phase, that is, $Li_{17}Ge_4$ and $Li_{16.38}Ge_4$ ($Li_{4.1}Ge$), crystallize isotypically with their Si counterparts and are analogous to $Li_{17}Pb_4$ and $Li_{4.11}Si$ structure types. Recently, the spatial arrangement of amorphous Li–Ge was confirmed with in situ ^{7}Li-NMR spectroscopy[67] and X-ray techniques.[68] The reversibility of Li lithiation/delithiation in Ge nanorods encapsulated by multiwall CNTs during cycling is regarded as strong support for the co-existence of amorphous and crystalline Li–Ge phases. The high capacity may be related to electrically driven, metastable, over-lithiated Li–Ge alloys existing within the structure (Figure 2a).[67] Other interesting complex lithiation characteristics have been observed, such as the local transformation of Li_7Ge_3 to Li_7Ge_2 due to the gradual breakage of Ge−Ge bonds among the Ge–Ge dimers (dumbbells) upon lithiation. Crystalline $Li_{15}Ge_4$ then grows, with an overlithiated phase of $Li_{15+\delta}Ge_4$ being formed at the end of discharge.[69] A recent theoretical study proposed Li_7Ge_3 to be the most stable composition in the Li–Ge phase diagram.[65]

The structural stability of the physical electrode is essential to maintain the high reversible capacity of the Ge electrode. Consequently, understanding and improving on this point has also received much attention. Strain/stress engineering of durable high-rate electrodes and energy harvesting through mechanical motion can be achieved by the coupled effects of lithiation kinetics and mechanical stress in electrochemical cycling (Figure 2b).[70] The long-range structural stability was preliminarily explored by several techniques. Germanium nanoparticles remained robust during cycling without any visible cracking as reported by Liang, et al.[71] Significant size-dependent characteristics were found for Ge particles during cycling as suggested by Weker, et al.[72] Only Ge particles with diameters larger than a few microns display cracks during cycling. Small Ge particles experience volume expansion and cracking before their larger counterparts but rapidly lose electrical contact.

The above-mentioned achievements have provided only a basic understanding of Ge-based electrode materials. The

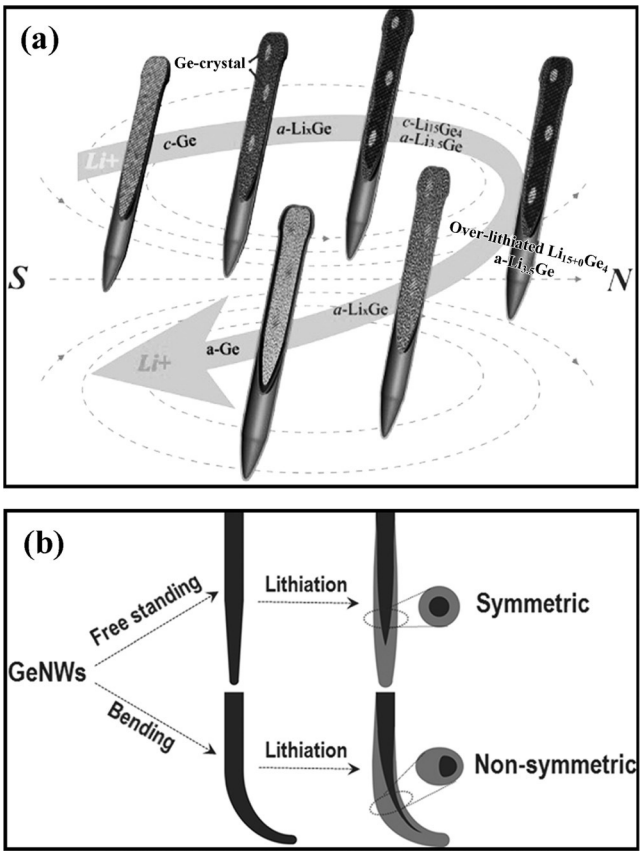

Figure 2. a) structural rearrangement and phase evolution of various Li–Ge alloy phases during (de)alloying reactions with lithium. Reproduced with permission from Ref. [67] Copyright 2015 The American Chemical Society. b) The evidence of controlled lithiation in germanium nanowires (GeNWs) through external bending. Reproduced with permission from Ref. [70] Copyright 2014 The American Chemical Society.

exact cause of the Li-storage capability and the relationship to the phase transition of Li-Ge alloys during cycling remain unclear. Next, attention will be given to the Li-cycling characteristics of Ge-based electrodes, and the influence of synthesis routes, morphologies, and structures on the electrochemical performances.

2.2. Pristine Ge for LIBs

2.2.1. Ge Nanoparticles for LIBs

In this Section, Ge nanoparticle (or nanowire) electrodes prepared via conventional slurry-casting processes are reviewed. Recently, hydrogen-reduced micro-sized Ge powders, exhibiting a specific capacity of approximately 1500 mA h g^{-1} after 40 cycles at 50 mA g^{-1}, have been reported by Ke et al. (Figure 3)[73] In another report, hydrogen-reduced Ge microcubes afforded a reversible capacity of 1250 mA h g^{-1} up to 200 cycles at 0.1 C with good retention of morphology .[74] Moreover, Ge microcubes are advantageous over micro-sized Ge powders for long-term cycling performance.

Efforts to resolve the issue of performance stability during long-term cycling under large current rates have been of particular focus for Ge electrodes. In 2010, long-range-ordered 3D porous Ge nanoparticles, prepared using a SiO_2 template, afforded a remarkable capacity of 1415 mA h g^{-1} up to 100 cycles at 1 C.[75] Subsequently, a 3D macroporous Ge particle electrode, produced by the magnesiothermic reduction method by Jia et al.,[76] has afforded not only a high reversible capacity of 1131 mA h g^{-1} at 1 C after 200 cycles, but also a high capacity of 717 mA h g^{-1} at 5 C (Figure 4). The performance characteristics agree with earlier results based on solution-grown Ge nanowires[77] (e.g., a reversible capacity of 1248 mA h g^{-1} after 100 cycles and capacity of 600 mA h g^{-1} after 1200 cycles at 1 C).

2.2.2. Binder-Free Ge Nanostructures for LIBs

To date, the in situ growth of Ge nanowires on metal substrates (binder-free electrodes) has received much interest due to their strain relaxation ability, good material durability, short Li diffusion distance, and compact electrical contact.[78,79]

2.2.2.1. VLS Growth

VLS growth is a viable way to produce Ge nanowires. In earlier works, the electrochemical performances of Ge electrodes have been investigated for use as the anode material of LIBs.[51,80] As early as 2008, Ge nanowire electrodes[78] fabricated by VLS growth on metallic current collector substrates have demonstrated a discharge capacity of 1141 mA h g^{-1} over 20 cycles at a rate of C/20. Subsequently, larger current densities were applied to clarify the influence

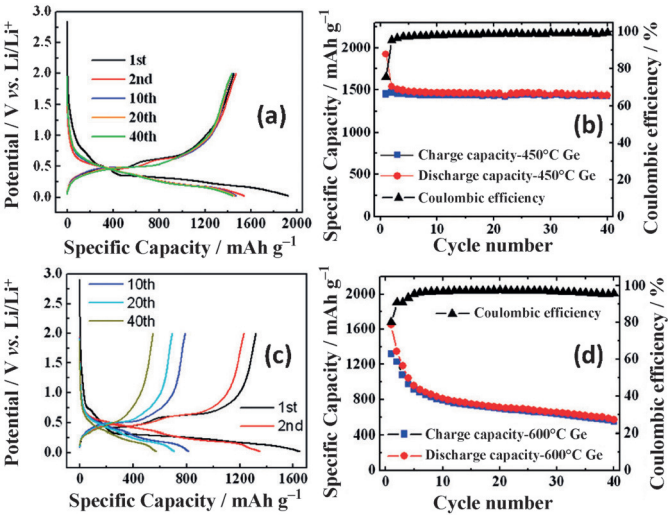

Figure 3. Electrochemical properties bulk Ge electrodes prepared from the thermal reduction of GeO_2 at 450 °C (a) and (b) and 600 °C (c) and (d). a) Voltage profile of the electrode reduced at 450 °C, b) specific capacity versus cycle number of the electrode reduced at 450 °C, c) voltage profile of the electrode reduced at 600 °C, and d) specific capacity versus cycle number of the electrode reduced at 600 °C. The charge-discharge current density was 50 mA g^{-1}. Reproduced with permission from Ref. [73] Copyright 2014 The Royal Society of Chemistry.

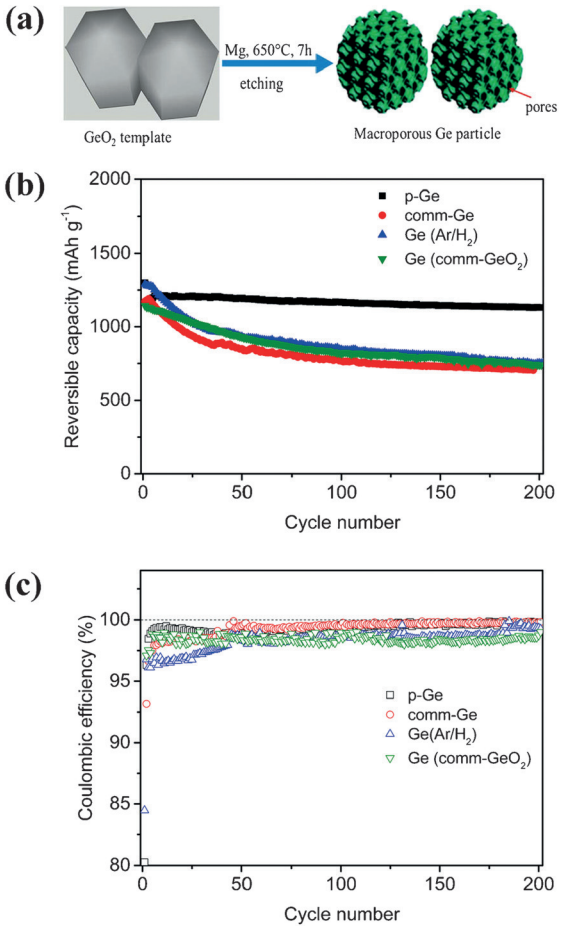

Figure 4. a) Schematic illustration of the preparation process of the porous germanium anode material by magnesiothermic reduction of GeO_2. b) Delithiation capacity curves and c) Coulombic efficiency curves of the constant current cycling of Ge-based electrodes, including *p*-Ge, commercial Ge, Ge(Ar/H_2) (reduced in an Ar/H_2 (95/5 vol %) atmosphere), and Ge(comm-GeO_2) (Ge prepared from commercial GeO_2) at 0.1 C (1st cycle) and 1 C (following cycles). Cut-off voltages: 0.01 and 1.5 V. Reproduced with permission from Ref. [76] Copyright 2014 The American Chemical Society.

of current density on reversible capacity. The Ge/Sn thermal co-evaporation method was employed to synthesize single crystalline Ge nanowires sheathed within a thin amorphous germanium suboxide (GeO_x) layer.[81] The self-supported Ge nanowire electrodes showed excellent capacity characteristics with little fading upon cycling (0.01 % per cycle; a capacity of 900 mA h g^{-1} at 1 C rate). In addition, high capacity stability is observed in research reported by Kennedy et al. (Scheme 3)[82] in which capacities of 900 mA h g^{-1} after 1100 cycles at 0.5 C are obtained. The high performance is attributed to the growth of the Ge nanowires into a continuous porous network.

Moreover, crystalline Ge nanowire films produced by an electrochemical liquid–liquid–solid (ec-LLS) growth process[79] supported a stable discharge capacity of 973 mA h g^{-1} at 1 C (i.e., 1624 mA g^{-1}) after 20 cycles. The specific capacity of a similar ion beam-mixed Ge electrode ultimately reached 1500 mA h g^{-1} at cycling rates of 0.2 C–1.6 C after 25 cycles.[80]

2.2.2.2. *Electrodeposition and Other Techniques*

In an interesting work, ionic-liquid electrodeposition was used to produce three-dimensional ordered macroporous (3DOM) films at room temperature.[83] The 3D ordered macroporous Ge delivered a reversible capacity of 1024 mA h g^{-1} and a capacity retention of 844 mA h g^{-1} after 50 cycles at 0.2 C. Ge nanotube array anodes, prepared by template-assisted electro-deposition from an ionic liquid had a capacity retention of 98 % relative to the 50th cycle (1025 mA h g^{-1}) after 250 cycles at 0.2 C. In another study, germanium deposited on electrodeposited nickel nanocone-arrays by high frequency plasma enhanced chemical vapor deposition (CVD)[84] exhibited a reversible specific capacity of 468 mA h g^{-1} at a rate of 0.5 C after 50 cycles.

In addition to the as-mentioned crystalline Ge nanowires, amorphous Ge nanotubes have also been reported.[85] Amorphous Ge nanotubes, directly synthesized on metallic current collector substrates via a template technique, delivered reversible capacities of around 1300 mA h g^{-1} at 0.05 C (1 C = 1600 mA h g^{-1}) after 20 cycles and retained capacities as high as 700 mA h g^{-1} at 2 C with columbic efficiencies over 99 %. Dual-active Sn/Ge nanowire arrays, prepared via solvent-vapor-growth (SVG), exhibited capacities greater than 1000 mA h g^{-1} after 50 cycles at 0.5 C (1245 mA g^{-1} for Sn seeded Si and 640 mA g^{-1} for Sn seeded Ge).[86]

The high first discharge/charge capacities of binder-free Ge electrodes were commendable. The long-term cycling characteristics are expected to meet the realistic requirements for Ge anode materials.

For battery applications, having large current discharging/charging capabilities are essential for commercial applications. In general, under low current densities of 0.1 C–0.5 C, the reversible capacities of binder-free Ge electrodes typically fall in the range of 900–1200 mA h g^{-1} after 200–1100 cycles.[82,87] Moreover, the Ge nanowires (binder-free) prepared by Mullane et al.[88] exhibited a high rate stability with a discharge capacity of 800 mA h g^{-1} at a rate as high as 10 C.

An antimony-wrapped-germanium nanowire produced a reversible capacity of more than 1000 mA h g^{-1} over 400 cycles with minimal capacity fading at 40 C (40 000 mA g^{-1}). This remarkable rate stability is attributed to the core–shell structure of the Ge–Sb nanowires.[89] However, a greater understanding of the structural and chemical consequences of core–shell structures and the contribution of Sb requires further investigation.

In essence, the alloying–dealloying reaction is the root cause of unavoidable volume expansion and electrochemical pulverization of active materials in electrodes. So far, the benefits of binder-free electrodes have been considered. The second route is through nanostructuring Ge materials which will be addressed in the following section. The third route to deal with the pulverization of pristine Ge electrodes during Li-cycling involves the introduction of second phase oxides to accommodate the volume expansion. Even though there are few reports concerning nanostructured Ge materials, a few examples are available and worth detailing in brief. Ge coated lithiated-CuO nanorods synthesized via vacuum evaporation gave a capacity retention above 95 % after 100 cycles at

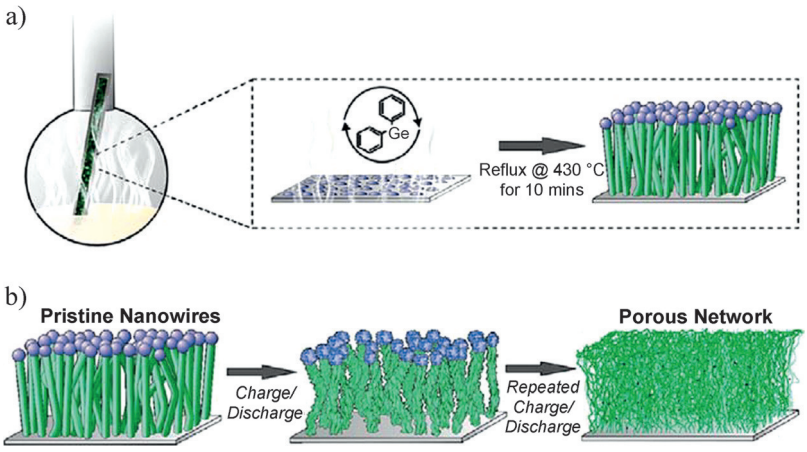

Scheme 3. a) Schematic illustration of the synthetic method used for NW growth. A pretreated stainless-steel substrate is placed in the vapor phase of a high boiling point solvent via a simple glassware-based setup. The temperature of the flask is ramped to 430 °C before injection of the germanium-based precursor. Growth proceeds via the well-established VLS mechanism. b) Schematic representation of the cumulative effect of cycling on the NW architecture. The pristine Ge NW array is transformed into a porous, interconnected network of active material as a consequence of the charge/discharge process. The transformation occurs over the first 100 cycles. Reproduced with permission from Ref. [82], Copyright 2014 The American Chemical Society.

a current density of 1000 $mA\,g^{-1}$.[90] In another instance, TiO_2@Ge core–shell nanorod arrays, produced via a hydrothermal method followed by radio frequency magnetron sputtering, exhibited a long-term cycling stability (700.3 $mA\,h\,g^{-1}$) at 5000 $mA\,g^{-1}$ after 600 cycles.[91] Clearly, more research into nanostructured Ge materials is warranted. Success in developing useful nanostructured materials for energy applications can be seen in graphene-based electrode research and titanium-based solar cell research.

Recently Ge/$LiCoO_2$ full-cells,[92] utilizing germanium-coated cobalt oxide as the anode material, have demonstrated high energy densities of 475 $W\,h\,kg^{-1}$ and high power densities of 6587 $W\,kg^{-1}$ (Figure 5). With a reasonable target capacity of 180–200 $W\,h\,kg^{-1}$,[4a] it is not only possible to meet the necessary immediate device performance requirements but also exceed them in the near future.

In summary, pristine Ge nanowires and nanotubes have emerged as promising anode materials for LIBs owing to their excellent electrochemical performance. However, the particular structure and morphology can play a major role in dictating the performance of pristine Ge materials over long working lifetimes. As demonstrated in previous work, improved cycle life of Ge electrodes can be attributed to the porous structure,[76] fast diffusion of Li^+, and amorphous Ge phase.[87] The porous structure and the short diffusion path of pristine Ge materials may be an acceptable theory for explaining the short-term cycling performance of Ge-based electrodes. However, it is insufficient as the sole explanation for the long-cycling performances of Ge-based electrodes. This is due to the fact that the pristine porous structure will also eventually collapse regardless of the porosity after long-term cycling as a result of the strong alloying–dealloying reaction. Two factors may be instrumental for improving the performance of pristine Ge-based electrodes: 1) The addition of carbonaceous materials which can enter into the voids of nanostructured Ge and act as an effective buffer to accommodate volume expansion during cycling; and 2) the presence and distribution of amorphous Ge.[63,64,67,69] An understanding of the Li-storage mechanism of pristine germanium is still not fully understood. Investigations into more complex hybrid structures will help shed light on the details of the mechanism while also boosting the desired performance characteristics.

2.3. Germanium–Carbon Hybrids

2.3.1. Germanium–Graphene Hybrids

To relieve the volume change of metal electrode materials, several strategies, including nanostructuring and the incorporation of a buffer layer such as carbon matrix, have been developed. Graphene has attracted growing attention owing to its large specific surface area (2630 $m^2\,g^{-1}$),[93] excellent electron mobility (ca. 15000 $cm^2\,V^{-1}\,s^{-1}$ at

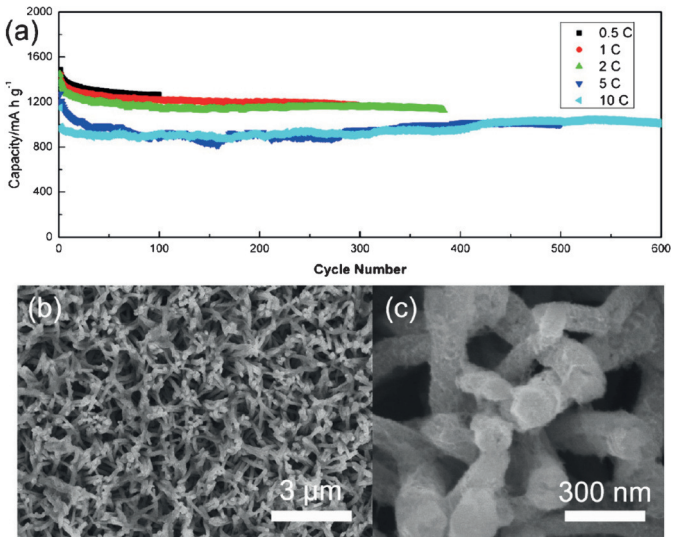

Figure 5. a) Galvanostatic discharge/charge cycles at 0.5, 1, 2, 5, and 10 C. b),c) SEM images of the coaxial Ge/Co_3O_4 nanorod array electrode after 100 cycles at 0.5 C. Reproduced with permission from Ref. [92] Copyright 2015 The American Chemical Society.

300 K),[94] high thermal conductivity (ca. 3000 $W\,mK^{-1}$ at ambient temperature),[95] and planar sp^2-hybridized carbon framework.[96] This popular carbon allotrope is often utilized as a matrix to support inorganic-based anode materials,[23,97–100] and is believed to maintain higher reversible capacities for the active materials it supports.[101,102] Recent investigations into sheet-like Sb/graphene hybrids[27] and Ni@graphene yolk@shell structures have supported this idea. For example, a first discharge (Li-uptake) capacity of 1034 $mA\,h\,g^{-1}$ and a stable cycling capacity of 490 $mA\,h\,g^{-1}$

after 100 cycles at 1000 mA g^{-1} was measured for Sb/graphene[27] and Ni@graphene,[103] respectively.

A recent Review summed up six different structure models of graphene and inorganic nanoparticles composites, and showed the channels for Li insertion/release thereby providing a crucial reference for future work.[104]

2.3.1.1. Anchored Model

This is the most common structure for graphene-supported composites. In the anchored model, electrochemically active nanoparticles are anchored on the surface of graphene, which is an inactive component.[104] In 2012, in situ sodium-reduced Ge nanoparticle/graphene nanocomposites were reported to exhibit a reversible capacity of 532 mA h g^{-1} after 15 cycles at 200 mA g^{-1}.[105] Subsequently, Ge/reduced graphene oxide (rGO) nanocomposites produced via solvothermal treatment followed by hydrogen-reduction showed improved reversible capacities of 690 mA h g^{-1} at 2000 mA g^{-1} after 150 cycles.[106]

A promising route to improve the Li cycling performance of LIBs is the chemical functionalization of graphene. This can enable strong chemical binding between active materials (metal nanostructures) and functional groups in graphene and thereby immobilize the metal into a 2D or 3D graphene composite. A sponge-like N-doped graphene/hydrogen-reduced germanium quantum dot material (Ge/GN sponge) produced a capacity of 1258 mA h g^{-1} after 50 charge/discharge cycles at 100 mA g^{-1}.[107] Amphiphilic polymer-coated rGO-Ge NPs (PSS-rGO-Ge NPs)[108] produced via an aqueous solution method delivered a reversible capacity of 760 mA h g^{-1} after 80 cycles under a current density of 50 mA g^{-1}.

Considering that the chemical binding between Ge and carbonaceous materials is similar to elements, such as N[55,109] and S,[110] other matrix materials besides graphene are also reviewed briefly. Metal–polymer electrode materials are an interesting alternative approach in which the matrix is also a binder of sorts that can deform and accommodate volume expansion. Recently, a nano-Ge/polypyrrole composite[111] produced a discharge capacity of 1014 mA h g^{-1} after 50 cycles at 0.2 C rate (based on the Ge). Ge/cyclized-polyacrylonitrile (PAN) produced a discharge capacity of 700 mA h g^{-1} after 100 cycles at 1 C.[55] Polymer-decorated Ge nanoparticles may provide a lower capacity because of the large molecular weight of polymer. Consequently, matrix materials with smaller molecule weights appear to be more promising. Light-weight N-doped carbon can also be combined with Ge via Ge–N binding[109] (between Ge nanoparticles and the carbon matrix) to produce a 3D N-doped carbon/Ge composite. The composite presents a porous structure which should effectively alleviate the volume expansion of Ge particles during Li-cycling. As a result, capacities as high as 1240.3 mA h g^{-1} at 100 mA g^{-1} and 813.4 mA h g^{-1} at 500 mA g^{-1} after 90 cycles have been reported[109] (Figure 6). Interestingly, Ge nanowires chemically decorated with dodecanethiol exhibited excellent electrochemical characteristics[110] (a reversible specific capacity of 1130 mA h g^{-1} at a rate of 0.1 C after 100 cycles). Moreover, full cells using the prepared Ge nanowire anode and a $LiFePO_4$ cathode could successfully drive light-emitting-diodes (LEDs) and audio devices.

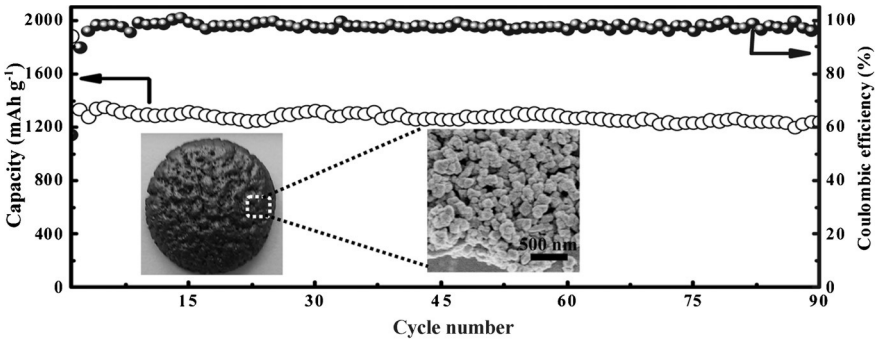

Figure 6. Cycling performance and the corresponding Coulombic efficiency of the typical Ge@C-N electrode at 100 mA g^{-1}. Inset: the FE-SEM (FE = field emission) images of the typical Ge@C-N hybrid. Reproduced with permission from Ref. [109] Copyright 2014 The American Chemical Society.

Anchored germanium should deliver stable capacity performance. However, it is unclear how to build high-density and strong chemical bonds between germanium and graphene due to the fact that germanium inherently lacks surface functional groups.

2.3.1.2. Wrapped, Sandwich-like, and Encapsulated Models

CVD is a practical approach to produce wrapped or sandwich-like graphene/Ge composites.[112] A sandwich-like Ge-graphene nanocomposite (45.3 wt% Ge) prepared via CVD[113] displayed a stable long-term cycling performance with a capacity of 675 mA h g^{-1} after 400 cycles at 400 mA g^{-1}. This is attributed to the uniform distribution of high-quality Ge particles embedded in a flexible graphene framework. A similar 3D Ge@graphene vertically aligned graphene (VAGN),[114] where Ge nanoparticles are wrapped and uniformly distributed on vertically aligned graphene (VAGN) via microwave plasma enhanced chemical vapor deposition (MPECVD), showed a Li-storage capability of 1014 mA h g^{-1} after 90 cycles at 260 mA g^{-1}. Notably, the electrode retained a capacity of 420 mA h g^{-1} at 13000 mA g^{-1}. In another related nanostructured material, graphene-wrapped Ge NWs afforded a high specific capacity of 1059 mA h g^{-1} at 4.0 C and a long cycle life of 200 cycles (Figure 7).[112] Above data seem to suggest that Ge nanoparticles combined with graphene, in a wrapped or sandwich-like structure, can achieve a stable reversible capacity of around 1000 mA h g^{-1} at various current densities over long-cycling. These three properties are the ultimate goal in energy storage devices and any devices which show promise at delivering all of them should be aggressively investigated.

In addition to the CVD method, other routes can be utilized to produce 3D structured Ge-graphene composites. Some other alternatives are included in this paragraph.

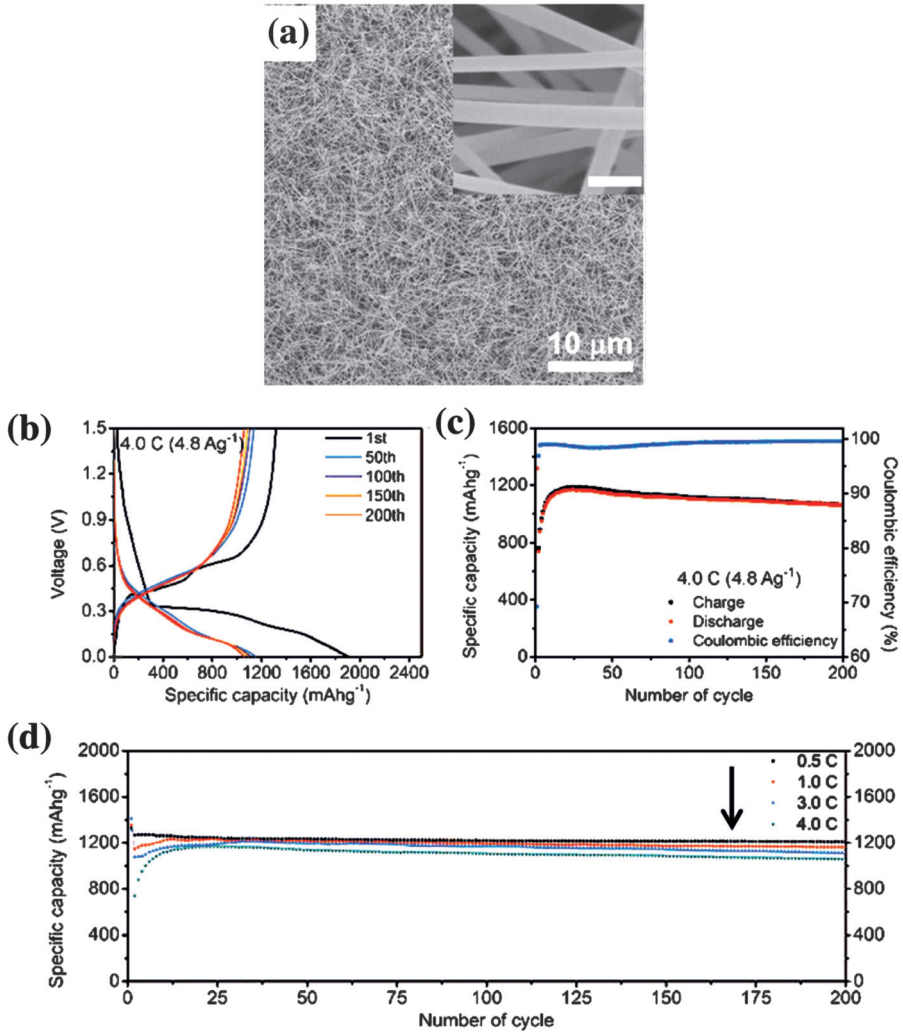

Figure 7. a) SEM image of as-grown Ge NWs. Scale bar in inset is 200 nm. b) Voltage profiles of a GN/Ge NW between 0.001 and 1.5 V at a rate of 4.0 C. c) Cycle performance of a GN/Ge NW and Coulombic efficiency at a rate of 4.0 C. d) Cycle performance of a GN/Ge NW at each C-rate from 0.5 to 4.0 C discharge). In the first cycle, the half-cell was charged and discharged at a rate of 0.05 C. Reproduced with permission from Ref. [112] Copyright 2013 Wiley-VCH.

Chemical-reduction has been used to distribute Ge nanoparticles on or between graphene nanosheets.[115] The resulting 3D composite materials maintained a capacity of about 832 mA h g^{-1} at 160 mA g^{-1} after 50 cycles. In another study, an interesting sponge-like structure composed of crystalline Ge particles encapsulated by graphene and amorphous carbon was produced through hydrogen reduction.[107] This electrode produced a reversible capacity of 1258 mA h g^{-1} after 50 cycles at 100 mA g^{-1}. The improved Li-storage capability was attributed to a pore memory effect and a highly conductive 3D N-doped graphene matrix. It is worth noting that physical routes such as discharge plasma can also play a significant role in forming Ge@few-layer graphene sheet nanocomposites[116] which can deliver a capacity of 846 mA h g^{-1} and a retention of 86% after 50 cycles at a rate of 0.4 C.

Graphene/Ge composites, with wrapped or sandwich-like structures, have demonstrated stable capacities (ca. 1000 mA h g^{-1}) and cycle characteristics. However, it remains challenging to create a uniform outer graphene layer at a low cost. In addition, forming strong and uniformly-dispersed chemical bonds between active Ge materials and graphene remains essentially a random/heuristic process. In the next few paragraphs, the focus is shifted to comparable structures in which Ge has improved chances to make close and intimate contact with graphene.

The reversible capacity of core–shell germanium-reduced graphene oxide (Ge-rGO) produced via sonication remained at 1100 mA h g^{-1} after 50 cycles at 0.1 C.[54] This is larger than that of Ge nanocrystals (800 mA h g^{-1}) due to the protective effect of surface carbon layers. Some special routes such as arc-discharged-graphene-encapsulated Ge nanowires[117] are also of interest. These Ge@graphene composites are composed of a graphene sheath and a metallic Ge nanowire core which affords a reversible specific capacity of 1400 mA h g^{-1} after 50 cycles at a current density of 1600 mA g^{-1}. It is clear that core–shell Ge/graphene composites deliver highly stable capacities. However, more in-depth investigations relating the structure and performance characteristics of such nanocomposites are required. Indeed, early results are promising. But they must be better understood and also demonstrated to be reproducible and reliable for each combination. In addition to sheet-like graphene, amorphous carbon has also been investigated for use in Ge nanocomposites anode materials.

2.3.2. *Ge and Amorphous Carbon*

Amorphous carbon is an inexpensive, frequently-used carbonaceous material which is easy to produce in industrial quantities. In LIB applications, amorphous carbon is used to produce a conductive compact outer-layer on the surface of Ge NPs which not only serves as a buffer layer to accommodate the volume expansion of Ge during cycling but also contributes to the formation of a stable solid-electrolyte-interface (SEI) layer. There are several synthesis routes available to put a carbonaceous layer around nanoparticles. It's important to understand the variation in the coverage and uniformity. These two properties contribute to the overall ability of different carbon coatings to accommodate volume changes.

2.3.2.1. Pyrolysis of Polymers

Many different polymers are amenable to pyrolytic (carbonization) reactions and can be used to coat the surface of active species. The strong adherence between Ge and the polymer leads to a strong and high quality amorphous carbon layer with large specific areas on the surface of the Ge nanoparticles. Therefore, pyrolysis of polymer-coated nanoparticles is an attractive approach for alleviating the problem of volume expansion during Li-cycling and can have a positive impact on the electrochemical performance of Ge-based anodes.

As early as 2008, carbon-encapsulated Ge nanoparticles,[118] produced via solid-state pyrolysis of an intermediate PTA-Ge thermally polymerized from tetra-allylgermane, demonstrated a first charge capacity of 923 $mA\,h\,g^{-1}$ at a current density of 150 $mA\,g^{-1}$. (Note: Tetra-allylgermane (TA-Ge) was polymerized to PTA-Ge about 250 °C in an argon atmosphere[118,119]) Subsequently, high reversible capacities were reported in Ge NP-carbon hybrid anodes via pyrolysis of poly(styrene-b-isoprene).[120] A high Li-insertion capacity of $1600 \pm 50\ mA\,h\,g^{-1}$ up to 50 cycles at 1 C was observed. Subsequently, a discharge capacity of around 770 $mA\,h\,g^{-1}$ after 500 cycles at 10 C was observed in carbon-encapsulated Ge and GeO_x nanowires by pyrolysis of organic–inorganic hybrids.[121] This improved rate performance and enhanced lifetime is promising.

2.3.2.2. Thermal Decomposition

The sol–gel technique is a well-established strategy to produce nanoparticles. As a representative example, thermal decomposition of Ge-citrate complex can produce nanometer-sized Ge crystallites interconnected by carbon which possesses a high porosity.[122] Resulting anodes showed an almost 98.8 % capacity retention (1232 $mA\,h\,g^{-1}$) even after 1000 cycles at a rate of 0.5 C. Comparable results have also been reported elsewhere.[123,124] In brief, some of their performance characteristics are as follows. In one study a discharge capacity of 1099 $mA\,h\,g^{-1}$ at 0.1 C after 100 cycles was obtained for mesoporous Ge@C spheres produced by thermal decomposition of Ge-catechol complex (Figure 8).[123] Recently, high capacity retention under long-term cycling has been observed for Ge-carbon hybrid nanoparticles via reduction and carbonization of germanium-chelate complex, that is, 895 $mA\,h\,g^{-1}$ over 2000 cycles at a rate of 2 C was observed.[125] In another study, a high specific capacity of 1360 $mA\,h\,g^{-1}$ at 1 C was reported for a carbon-filled Ge hybrid produced via thermal evaporation of Ge powders followed by decomposition of the citric acid.[124]

In summary, long-term reversible capacities at large current densities can be achieved for Ge/C nanoparticles produced via simple thermal decomposition methods. Such techniques offer more uniform carbon coverage/distribution and nano-crystalline Ge particles. More research should be devoted to yielding Ge/C composites with different morphologies and 3D structures through sol–gel processes.

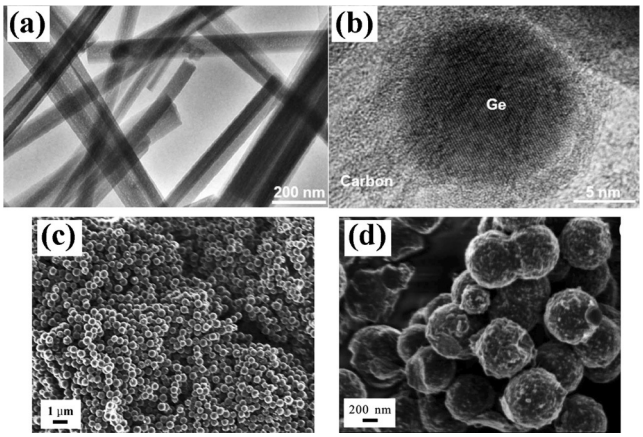

Figure 8. a),b) TEM images of Ge/C nanowires. Reproduced with permission from Ref. [121] Copyright 2014 The American Chemical Society. c),d) SEM images of mesoporous Ge@C spheres. Reproduced with permission from Ref. [123] Copyright 2014 The Royal Society of Chemistry.

2.3.2.3. Chemical Vapor Deposition

CVD has also been shown to be a feasible way to produce amorphous carbon coatings.[126] In 2011, carbon-sheathed single crystalline Ge nanowires produced by a solid–liquid solution (SLS) method followed by CVD were reported.[127] The resulting anode was responsible for a high reversible charge capacity of 963 $mA\,h\,g^{-1}$ at a rate of 0.5 C (i.e., 400 $mA\,g^{-1}$) after 100 cycles. Some comparable results have been reported for Ge-3D graphene structures made by CVD[23] and Ge@C core–shell structures made by microwave plasma chemical vapor deposition (MPCVD). These devices delivered reversible capacities of 1140 $mA\,h\,g^{-1}$ at 1/3 C over 100 cycles and 734 $mA\,h\,g^{-1}$ over 100 cycles at a current density of 800 $mA\,g^{-1}$.[128] Similar Ge@amorphous carbon nanocomposites produced via CVD gave large current densities of 600 $mA\,g^{-1}$over 200 cycles.[129]

2.3.2.4. Thermal Reduction

Thermal reduction, including magnesiothermic and hydric reactions, is commonly employed to produce Si/C anode materials.[130–132] Magnesiothermically reduced Ge particles can also be produced in an adapted process.[133,134] A porous Ge@C composite[133] produced by magnesiothermic reduction followed by acid corrosion delivered a reversible capacity of about 790 $mA\,h\,g^{-1}$ after 100 cycles at a rate of 0.2 C and reversible capacity of 440 $mA\,h\,g^{-1}$ at a high current density of 1800 $mA\,g^{-1}$. To facilitate magnesiothermic reduction, salt (NaCl) was also added as a heat scavenger to make nanoporous Si and Si/Ge composites.[134]

Compared with magnesiothermic-reduction, hydrogen reduction has the advantage of not requiring acid corrosion which makes the process more environmentally friendly.[135–139]

Another appealing feature of hydrogen-reduction is that different types of voids such as mesoporous hollow Ge[136] and porous amorphous Ge[140] can be obtained in Ge/C hybrids.

As a representative example, porous carbon–germanium nanowires (PC-Ge NW)[135] produced via SLS followed by hydrogen reduction gave a specific capacity of 789 mA h g^{-1} at the 50th cycle under a current density of 160 mA g^{-1}. Mesoporous hollow germanium@carbon nanostructures,[141] hierarchical micropore–mesopore carbon/Ge (C/Ge) hybrids,[137] and hollow carbon with encapsulated germanium (Ge@HCS; Figure 9)[138] have all shown similarly high reversible capacities, such as 1137 mA h g^{-1} after 200 cycles at a rate of 0.2 C,[141] 906 mA h g^{-1} at 600 mA g^{-1} after 50 cycles,[137] and about 1000 mA h g^{-1} up to 100 cycles at a rate of 0.4 C, respectively.[138]

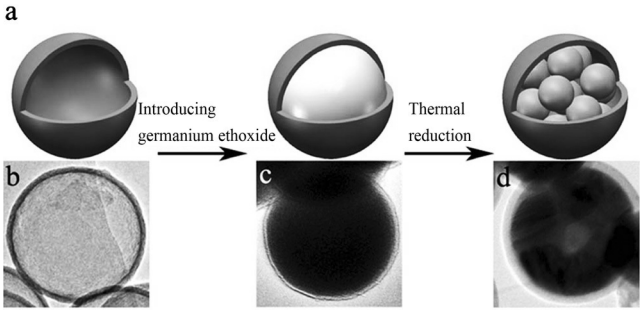

Figure 9. a) Schematic illustration of the incorporation of germanium into the hollow carbon spheres. TEM images of b) HCS, c) GeO_2@HCS, and d) Ge@HCS. Reproduced with permission from Ref. [138] Copyright 2015 The Royal Society of Chemistry.

In addition, two less-familiar methods have provided a more open design philosophy for synthesizing Ge@C hybrids. 1) Carbonization under an *n*-hexane atmosphere was capable of synthesizing Ge@C core–shell nanostructures[142] which produced a specific capacity of 985 mA h g^{-1} at a current density of 500 mA g^{-1} after 50 cycles; 2) The Ge–C composites, produced via a tandem plasma reaction method,[143] delivered a capacity of 980 mA h g^{-1} at 2000 mA g^{-1} with less than 2% capacity loss in up to 100 cycles.

It appears that compact carbon coatings on Ge@C nanostructures afford high Li-storage capabilities at large current densities and over long cycle times. The above-mentioned high-temperature processes have produced two notable features which are likely important for producing high performance anodes and LIB devices: 1) the excellent crystal phase of Ge, and 2) the highly porous microstructure into which amorphous carbon can be homogeneously distributed and thereby more effectively accommodate the volume expansion during repeated Li-cycling.

2.3.3. *Ge–CNT (CNF) Hybrids*

Carbon nanotubes (CNTs) are allotropes of carbon with a cylindrical nanostructure. They find applications in LIB electrode materials owing to their extraordinary thermal, mechanical, and electrical properties. CNTs can be categorized as single-walled (SWCNTs) and multi-walled nanotubes (MWCNTs). CNTs are generally employed as conducting agents which replace carbon black when used in the electrode of LIBs.

By early 2011, 3D freestanding electrodes[144] containing Ge-NPs prepared via a CVD process and SWCNT afforded a capacity of 983 mA h g^{-1} versus Li/Li^+ up to 3 V. Subsequently, the active role of SWCNT was confirmed by Forney et al.,[145] showing that SWCNT can significantly improve the specific capacity (1100 mA h g^{-1} with 1% SWCNT), rate performance (80% capacity retention at 1 C rate), and enhance the energy density in full-cell batteries by 20–25%. Recently, ionic liquids were also used to produce electrodeposited Ge-NPs-/CNT hybrid materials[146] that deliver a reversible capacity of 810 mA h g^{-1} after 100 cycles at 0.2 C.

The use of CNTs as current collectors is becoming competitive with traditional copper foil. By adopting vertically aligned CNT (VACNT) arrays as a 3D current collector on a Ge film, a high reversible capacity of 1314 mA h g^{-1} after 100 cycles at 0.2 C was observed.[147] Similar results are found in vertically aligned MWCNT/polycrystalline-Ge (via CVD) and MWCNT/amorphous-Ge (via radio frequency sputtering) materials.[148] The MWCNT/amorphous-Ge materials retained a specific capacity of 1096 mA h g^{-1} at a current density of 162 mA g^{-1} at the 100th cycle. A flexible paper-like electrode using Ge and CNT materials was produced via vacuum filtration.[149] Such an electrode, composed of 32% Ge and SWCNT, delivered a specific discharge capacity of 417 mA h g^{-1} after 40 cycles at a current density of 25 mA g^{-1}. Notably, the thermal safety of Ge-NP:SWCNT electrodes can be improved by developing a passivation layer of high surface-area SWCNTs.[150] Taking into account the recent progress in CNTs and the many low-cost synthetic methods available, it is likely that practical applications for Ge-CNT anode materials will become possible in the near future.

Carbon nanofibers (CNFs) are cylindrical nanostructures with graphene layers arranged as stacked cones, cups, or plates. Carbon nanofibers with graphene layers wrapped into perfect cylinders are called carbon nanotubes. Carbon nanofibers have also received increased attention for use as the matrix in the LIBs.[151] Even though Ge@CNF and Ge@C@CNF[152] encounter rapid capacity loss, flexible and self-supported Ge-CNFs (top panels in Figure 10)[153] consisting of Ge nanoparticles encapsulated in CNF by electrospinning technique achieved a reversible specific capacity of 1420 mA h g^{-1} after 100 cycles at 0.15 C. When cycled at 1 C, they still maintained a reversible specific capacity of 829 mA h g^{-1} after 250 cycles. In a related work, in situ grown germanium clusters were homogeneously encapsulated into porous nitrogen-doped carbon nanofibers (N-CNFs) to form Ge/N-CNFs hybrids.[154] This electrode material produced a reversible capacity of 1267 mA h g^{-1} after 50 cycles at a current density of 100 mA g^{-1}. In another reference,[155] graphite nanofibers (GNFs) were also used to produce a Ge NW/GNF composite which produced a specific capacity of about 1200 mA h g^{-1} after 30 cycles at 0.1 C.

In summary, the use of CNTs (or CNFs) can provide a stable nanoscale electrical network to support Ge NPs resulting in a hybrid three-dimensional electrode. Consequently, admirable electrochemical performance, around 1000–1400 mA h g^{-1} after 50–100 cycles at a current density

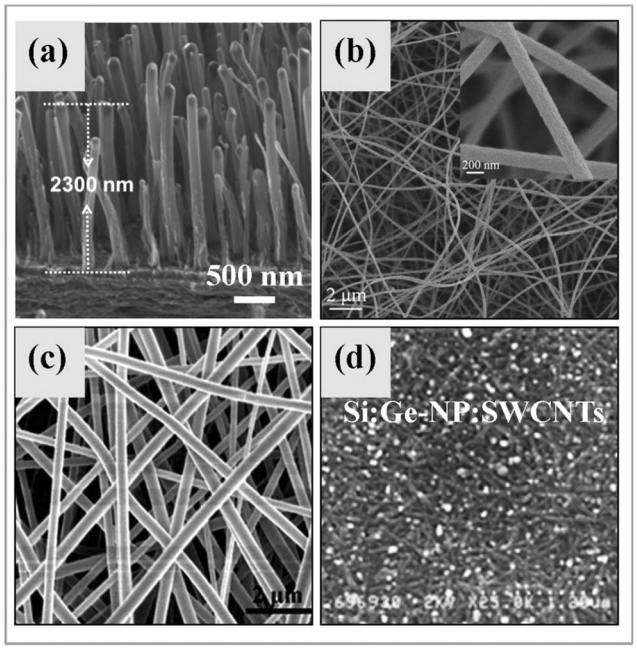

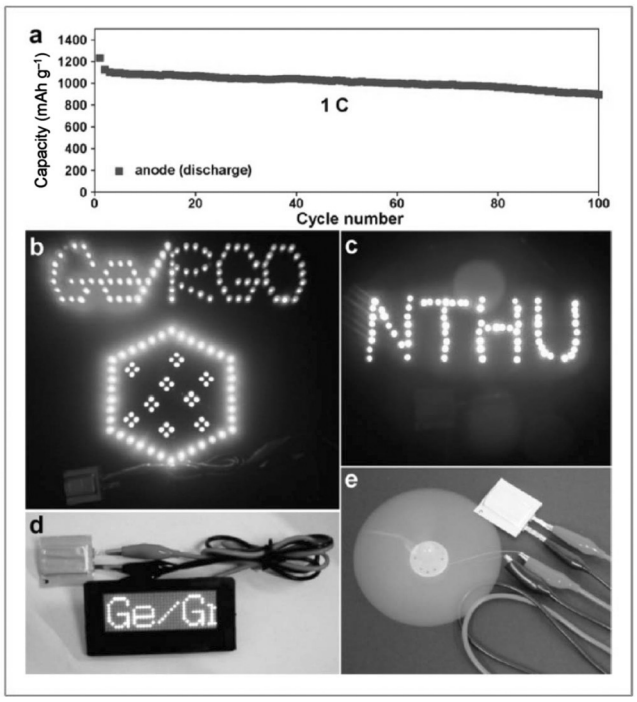

Figure 10. Top: typical morphologies: a) Side-view SEM image of as-grown VACNTs. Reproduced with permission from Ref. [147] Copyright 2014 Wiley-VCH. b) FE-SEM micrographs of nanofibers Ge@CNF nanofibers. Reproduced with permission from Ref. [153] Copyright 2014 The Royal Society of Chemistry. c) FE-SEM images of the as-spun EDA-Ge-PVP nanofibers (EDA = ethanediamine, PVP = polyvinylpyrrolidone),[154] and d) SEM images of Si-Ge-NP:SWCNT. Reproduced with permission from Ref. [150] Copyright 2013 Elsevier. Bottom: a) Discharge capacity of the Ge/RGO/C anode versus cycle number in a full cell with an $LiCoO_2$ cathode at a charge/discharge rate of 1 C between 2.5 and 4.2 V. Aluminum-pouch-type Li-ion batteries were used to power different electronic devices, including b) an LED array containing over 150 bulbs, c) blue LED bulbs, d) a scrolling LED marquee, and e) an electric fan. Reproduced with permission from Ref. [158] Copyright 2014 The American Chemical Society.

of about 100–200 $mA\,g^{-1}$, has been reported in Ge-CNTs (CNFs) composite electrodes. However, there are several obstacles when using CNTs (CNFs). First, CNTs must become cost competitive and producible on an industrial scale in order to compete with conventional conducting agents (carbon black) or collectors (copper foil). Second, accommodating the volume expansion of Ge metal during cycling with CNTs (CNFs) is also problematic because the unique tubular or fibrous structure of CNT/CNF can neither cover nor wrap the active materials. During cycling, it is probable that the active materials and CNTs/CNFTs become linked or entangled after they are electrochemically activated in unknown ways.[156] Therefore, what happens to the CNTs/CNTs seems to affect the active materials. A natural question then is to investigate more complex mixtures of active and carbonaceous materials to afford both volume expansion accommodation and improved device performance over long cycling periods.

2.3.4. *Dually Protected Ge Hybrids*

As mentioned in Sections 2.3.1 and 2.3.2, there is much evidence to support that both graphene and amorphous carbon can enhance the electrochemical activity and cycling stability in battery applications. Therefore, dual protection (i.e. mesoporous carbon and graphene) of Ge particles has also been considered for simultaneously improving the stability and properties.

As early as 2012, double-protection strategies have been investigated to improve the Li-cycling characteristics of Ge-based electrodes. A core–shell Ge@C/rGO nanocomposite showed excellent cycling performance (ca. 940 $mA\,h\,g^{-1}$ after 50 cycles at 50 $mA\,g^{-1}$) and rate capability (ca. 380 $mA\,h\,g^{-1}$ after 50 cycles at 3600 $mA\,g^{-1}$) in comparison to Ge@C nanoparticles (ca. 490 $mA\,h\,g^{-1}$ reversible capacity at a rate of 50 $mA\,h\,g^{-1}$).[157] Recently, Ge@CNF@C[152] composites exhibited a high capacity retention of 89% (553 $mA\,h\,g^{-1}$) at the 50th cycle under 50 $mA\,g^{-1}$ due to the structurally durable thorn-like Ge morphology and the additional CVD-prepared carbon confinement. Furthermore, dually protected Ge/rGO/C composites produced via hydrogen-reduction gave a capacity of 1332 $mA\,h\,g^{-1}$ (based on Ge nanoparticles) after 75 cycles at a rate of 0.2 C (bottom panels in Figure 10).[158] Subsequently, the assembled full-cell employing Ge/rGO/C as the anode and $LiCoO_2$ as the cathode could successfully illuminate an LED array, blue LED bulbs and a scrolling LED marquee. To date, research is fairly lacking for dual-protection hybrids. More efforts in this area are needed for establishing the relationship between the complex structure and electrochemical performance.

In summary, Ge has been widely investigated as an active material in anodes for LIBs. Several different structures and morphologies were produced via different synthetic routes in an attempt to meet the high electrochemical performance requirements of Ge-based electrodes including large rate capabilities and long-term cycling performance. Several additives have been combined with Ge to improve on one or several of the important performance metrics. Among them, graphene provides the most structural possibilities for Ge-based hybrids owing to its unique sheet-like structure.

Amorphous carbon has also been employed due to its low-cost and more intimate contact with the active material. Therefore, Ge/graphene and Ge/carbon hybrids have shown promise as anode materials for next-generation LIBs in different and complimentary ways.

Considering that the formation of Li–Ge alloys is the origin of the reversible capacity in the Ge-based materials during Li-cycling, it is necessary to address alloys of germanium with other metals that can be used to accommodate lithium cycling. The goal is to understand the nature of Li-cycling in a broader context, and simultaneously explore the possibility of Ge-based alloys as anode materials.

2.4. Germanium Alloys

Germanium possesses the ability to form alloys with many different metal and non-metal elements in varying compositions. Consequently, all the different alloys have different properties and varying utility as an anode material.[159] Several examples are detailed below. Binary Ge–Au alloys can be produced under hydrogen flow when heated to 960 °C. They show good casting and welding capabilities with Cu–Au alloys and gold. Another Ge–Cu alloy displays good hardness and corrosion resistance. As to the ternary alloys, Ge–Ti–Zr alloys may be used in welding of graphite and refractory metals. Of particular note are Si–Ge alloys, the most common Ge-based alloys, which have found increasingly active roles in thermoelectric devices[160] and advanced high-speed transistors[161] which are widely applied in high-frequency communication chips, car collision radar systems. and high performance local networks. In the following Sections, the unique applications of Ge-based alloys in next-generation energy-storage devices are reviewed.

Focusing on the Li-storage mechanism of alloys, Li–Zn–Tt (Tt = Ge or Sn) systems were investigated.[162] Band-structure calculations for $Li_3Zn_2Sn_4$ indicated that the phase was metallic, with a Fermi level at the flank of a pseudo-gap in the density of states (DOS) curve. The topological analysis of the electron localization function (ELF) showed covalent Sn–Sn bonding and lone-pair-like valence basins for the Sn atoms. Strong covalent Ge–Ge interactions were established in $Li_xLa_5Ge_3$,[163] which was formed by the incorporation of lithium atoms into octahedral voids of the La_5Ge_3 binary phase. The representative binary alloy phase diagrams are provided to highlight the corresponding characteristics associated with the different solid solutions (Figure 11).

2.4.1. Ge–Cu Alloys for LIBs

Acting as a fast-diffusion impurity in Ge, copper can form Cu–Ge alloys via the dissociation diffusion mechanism. As early as 2012, three-dimensional Cu–Ge core–shell nanowire array electrodes[164] produced via an RF-sputtering method displayed attractive reversible capacities (a reversible capacity of 1419 mA h g^{-1} at 0.5 C after 40 cycles and

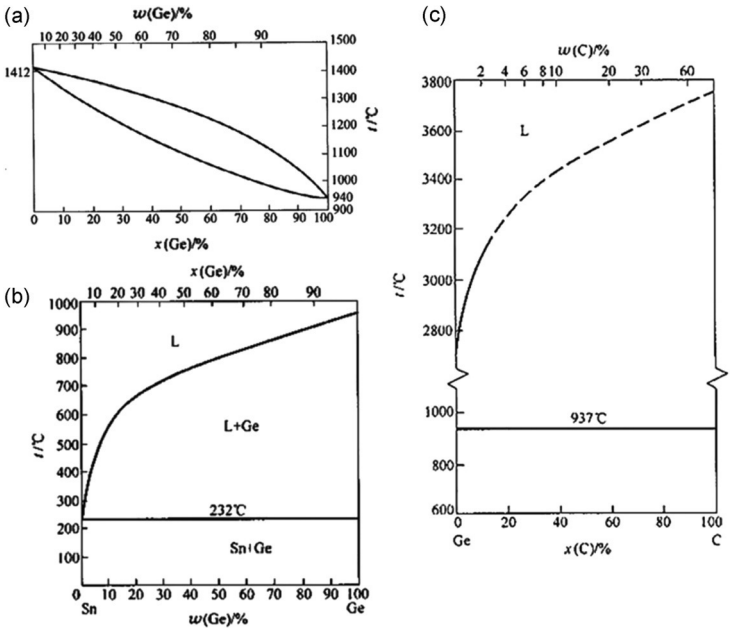

Figure 11. Binary alloy phase diagram of a) Ge–Si, b) Ge–Sn, and c) Ge–C.

734 mA h g^{-1} at 60 C after 80 cycles). However, relatively few reports have been made on such materials and the repeatability of such performance characteristics remains largely unverified. Similar reversible capacities have been established under much lower current densities in subsequent works. For example, Ge–Cu nanoparticles (Ge–Cu NPs) were fabricated by a gas-condensation method.[165] An observed reversible discharge capacity of 810 mA h g^{-1} at 0.2 C after 50 cycles was attributed to the multi-step lithiation/delithiation of $Li_{22}Ge_5$. In another study, a Ge–CNT–Cu monolith anode was produced by direct growth of Ge onto a CNT-coated Cu substrate. The resulting device produced a discharge capacity of 800 mA h g^{-1} after 100 cycles at a current density of 150 mA g^{-1}.[166] In brief, Cu–Ge alloys seem to be attractive due to their enhanced conductivity and their compatibility with current-collector materials. Cu–Ge alloy anodes are relatively new and require more fundamental structure–property relationship investigations.

2.4.2. Ge–Si Alloys for LIBs

First developed in 1955, Ge–Si alloys have been an essential semiconductor material but more recently have also shown utility as an anode material. Pure Si itself has served as an effective anode material in LIBs.[167,168] Subsequently, Ge has also attracted attention due to its large electronic conductivity (2.1 S m^{-1}; 1.6×10^{-3} S m^{-1} in silicon) and ionic diffusivity (6.25×10^{-12} cm^2 s^{-1}; 1.9×10^{-14} cm^2 s^{-1} in silicon).[169] An investigation into the reduced charge transfer resistance,[170] accounting for the interfacial Li^+ ion intake from the electrolyte, may be indicative of the key role of the Ge layer as an electron supplier. In Si–Ge alloys,[171] it is interesting to note that swelling appears only if the Ge concentration is above 90 % (already very high loading). These findings are a consequence of the void nucleation

governed by the starting material that determines the features of porous structures and growth mechanism.

It is reasonable to think that Ge–Si alloys should afford a more attractive electrochemical performance due to the combination of germanium (excellent electronic conductivity) and silicon (high capacity and low-cost) when used in LIBs. They are particularly attractive for all-solid-state Li-ion microbattery applications in on-chip power systems integrated into micro-electronic devices, such as micro-electronic/nano-electronic mechanical systems (M/NEMS) devices[172] or autonomous wireless microsystems where volume is a limiting factor.

RF/DC magnetron sputtering is commonly used to obtain Ge–Si thin films.[173] Such films displayed discharge capacities of 1981 $mA\,h\,g^{-1}$ and 1810 $mA\,h\,g^{-1}$ at a rate of 1.35 C (1.8 $mA\,cm^{-2}$), with a capacity retention of about 50% after 100 cycles. A reversible capacity of 1559 $mA\,h\,g^{-1}$ after 100 cycles at a current density of 600 $\mu A\,cm^{-2}$ has been observed in Si/Ge multi-layer cells fabricated by this magnetron sputtering approach.[174] After assembly in a full cell, the $Si_{0.84}Ge_{0.16}/LiCoO_2$ cell delivered a specific capacity of around 160 $mA\,h\,g^{-1}$ and a capacity retention of 52.4% after 100 cycles. Recently, Si–Ge nanorod (NR) arrays also produced via RF magnetron sputtering exhibited capacities of approximately 220 $\mu A\,h\,cm^{-2}$ after 60 cycles under a current density of 20 $\mu A\,cm^{-2}$ within the voltage window from 0.13 V to 2.0 V versus Li/Li^+ (Figure 12).[175]

Besides RF magnetron sputtering,[175] CVD can be used to precisely deposite Ge on Si arrays as well. In 2012, Si/Ge double-layered nanotube arrays (produced via CVD) demonstrated a first discharge capacity of 1746 $mA\,h\,g^{-1}$ at 0.2 C, and capacity retention of 85% after 50 cycles.[176] Subsequently, a 3D structured hexagonal bottle-like Si/Ge nanorod (NR) array composite was produced by Yue et al. (Scheme 4)[169] on a wafer scale and in a Si-compatible process (CVD: decomposition of GeH_4). The favorable structure and improved conductivity features of Ge/Si NR arrays are likely responsible for the capacity of 0.1 $mA\,h\,cm^{-2}$ up to 100 cycles at 300 $mA\,cm^{-2}$. Another interesting core–shell nanowire has also been constructed via CVD (using SiH_4 and GeH_4 as raw materials).[177] Such a Si–Ge heterogeneous nanostructure has afforded a first charge capacity of 1276 $mA\,h\,g^{-1}$ at rate of 0.2 C and a capacity retention of 72.4% after 50 cycles.

In summary, Ge–Si alloys provide a fairly stable electrochemical response because of the combination of the advantages inherent in both Ge and Si. However, there are several challenges remaining including how to make homogeneous alloys between Si and Ge. On the other hand, achieving a balance between cost and performance in Ge–Si alloys is also crucial.

2.4.3. Ge–Sn Alloys and Others for LIBs

Germanium can form numerous alloys with other metals including tin[178] and titanium (Figure 13 a,b).[179] Germanium-tin ($Ge_{1-x}Sn_x$) alloy nanocrystals were synthesized using a gas-phase laser photolysis reaction.[178] Incorporation of Sn ($x = 0.05$) significantly increases the capacity (1010 $mA\,h\,g^{-1}$ after 50 cycles)

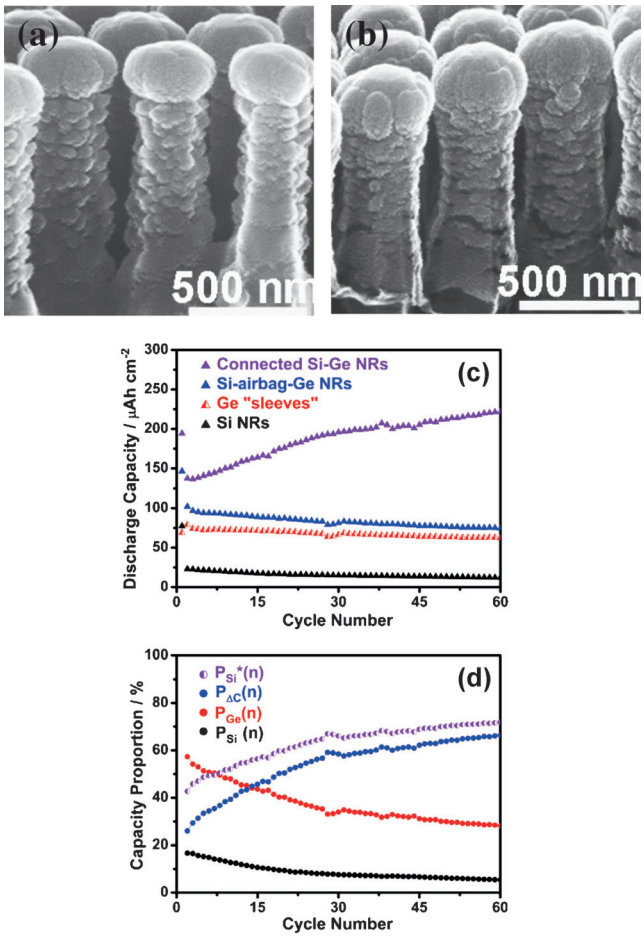

Figure 12. Top: Section-view SEM images of connected a) Si–Ge NRs, and b) Si-airbag-Ge NRs. Bottom: c) Discharge capacities of Si NRs, Ge "sleeves", Si-airbag-Ge NRs, and connected Si-Ge NRs electrodes under the current of 20 $\mu A\,cm^{-2}$ within the voltage window from 0.13 to 2.0 V versus Li/Li^+ until 60th cycle. d) Capacity proportions of the individual Si inner cores, Ge outer shells, increment caused by the specific connected core–shell structure, and the effective capacity of the Si inner cores in the connected Si–Ge NR anode during 1st to 60th cycles. Reproduced with permission from Ref. [175] Copyright 2014 The American Chemical Society.

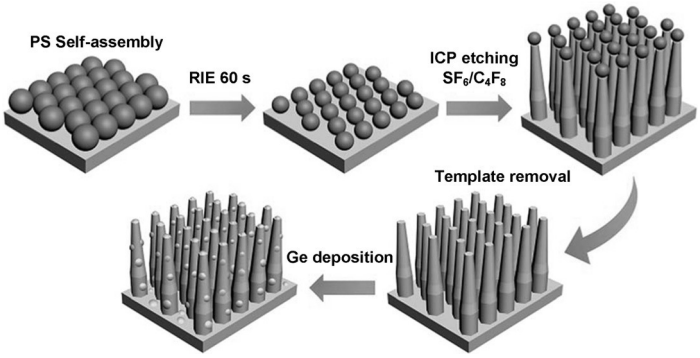

Scheme 4. Illustration of the fabrication processes of Si/Ge NR arrays. ICP = inductively coupled plasma, PS = polystyrene. Reproduced with permission from Ref. [169] Copyright 2014 The Royal Society of Chemistry.

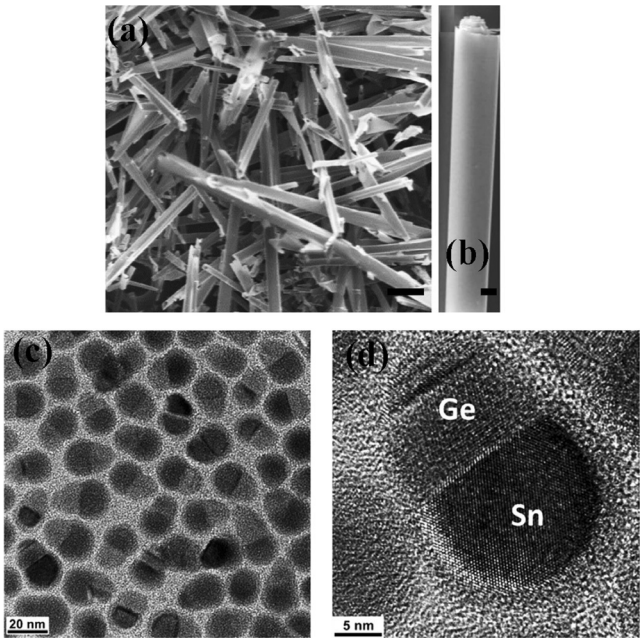

Figure 13. Typical morphologies of Ge-based alloys. a) A typical SEM image of the hybrid multilayer Ge/Ti microtubes formed by the strain-released method, scale bar: 10 μm. b) A magnified SEM image of a single rolled-up Ge/Ti microtube showing a cylindrical hollow structure composed of multilayer stacks, scale bar: 2 μm. Reproduced with permission from Ref. [179] Copyright 2013 Wiley-VCH. c) Low-resolution and d) high-resolution transmission electron microscopy (TEM) images of SnGe nanorods. Reproduced with permission from Ref. [181] Copyright 2014 The American Chemical Society.

and rate capability. Approximately the same reversible capacities could be achieved in various Sn–Ge alloys via several different approaches such as melt spinning[180] and SLS growth (Figure 13c,d).[181]

Sn–Ge alloys are believed to undergo a detectable phase transformation,[180] for example, from the crystalline Sn–Ge alloys to nanocrystalline Sn embedded in an amorphous Ge matrix, during Li-cycling. In addition, biphasic Janus structures in Sn–Ge alloys have been recently reported.[181,182]

Furthermore, there is a wealth of other binary (or ternary) alloys containing Ge that can be used in LIB anode materials.[183] For example, ultrathin Ti/Ge bilayer nanomembranes produced via electron-beam deposition are worth noting because of their capacity of 930 $mA\,h\,g^{-1}$ after 100 cycles at C/16.[179] In another example, with the help of a nonreactive glassy Li-Se-Ge phase, slurry-casted $Ge_{0.9}Se_{0.1}$ particle electrodes produced a reversible capacity of 800 $mA\,h\,g^{-1}$ for 900 cycles at a 1 C rate.[184] This is an especially promising result. Of note is amorphous ternary Si–Ge–Mo alloy films,[131] particularly $Si_{0.41}Ge_{0.34}Mo_{0.25}$ composites produced via RF/DC magnetron sputtering, which showed high specific capacities (1st charge: 1193 $mA\,h\,g^{-1}$), long cyclability (ca. 870 $mA\,h\,g^{-1}$ over 100 cycles), and good initial Coulombic efficiency (ca. 96%). Additionally, the $Si_{0.55}Ge_{0.22}Mo_{0.23}$ composite electrode displayed excellent cyclability with a high-energy density when coupled with a $LiCoO_2$ cathode. Other compositions are also likely to demonstrate advantageous properties for use in LIBs and other energy-storage devices.

In summary, Ge-based alloys, especially Ge–Si alloys, have shown great potential for anode materials in LIBs owing to their high specific capacity, low-cost, abundance, and controllable alloy compositions. However, the structural stability of alloy electrodes still needs to be verified under large current densities and long-term cycling conditions. Furthermore, accommodating the volume expansion still remains as a stubborn and unavoidable problem. Perhaps the incorporation of carbonaceous materials into alloy anode materials may serve to address the problem in the same way as for pure Ge-based metallic anodes. In addition to metallic alloys, compounds of germanium have been investigated for use in anodes. Such materials will be the focus of the next Section.

2.5. Germanium Compounds for LIBs

In 2009, lithium cycling of GeO_2, $MGeO_3$ (M = Cu, Fe, and Co), and $CuO{\cdot}GeO_2$ composites in the voltage range 0–3.0 V was discussed by Kim et al.[185] Subsequent work on GeO_2 films has since provided some insight into the influence of grain size on the electrochemical performance.[186] GeO_2 (10 nm) thin films possessed an initial capacity of 930 $mA\,h\,g^{-1}$ with 89% capacity retention after 100 cycles, compared with 455 $mA\,h\,g^{-1}$ with 53% capacity retention for GeO_2 (100 nm). Higher capacities were subsequently found in GeO_2 nanocrystals synthesized by gas phase laser photolysis (1100–1220 $mA\,h\,g^{-1}$ after 100 cycles at a current density of 160 $mA\,g^{-1}$).[187] The incorporation of graphene (and other carbonaceous materials) has also been investigated for germanium oxides. Of special note is the combination of amorphous GeO_x ($1.01 < x < 1.07$) and rGO which afforded a high reversible capacity of 1600 $mA\,h\,g^{-1}$ at 100 $mA\,g^{-1}$ and reversible capacity of 410 $mA\,h\,g^{-1}$ at 20000 $mA\,g^{-1}$ as reported by Lv et al.[188] In another study, GeO_2/Ge/C nanoparticles[189] delivered a high capacity of approximately 1650 $mA\,h\,g^{-1}$ at 1 C (i.e., 2100 $mA\,g^{-1}$) after 50 cycles as a result of the reversibility of the conversion reaction of GeO_2 and the presence of carbon which can accommodate the volume change to some extent.

In addition to oxygen compounds, sulfides and selenides of germanium are interesting potential anode materials. Both germanium sulfide (GeS) and germanium disulfide (GeS_2) adopt orthorhombic crystal systems (space groups are *Pnma*, *Fdd2*, respectively). In a typical example, gas-phase laser photolysis followed by thermal annealing can produce GeS and GeS_2 nanoparticles.[190] Crystalline GeS (c-GeS) nanoparticles afforded a capacity of 1010 $mA\,h\,g^{-1}$ after 100 cycles at 0.1 C. Interestingly, both amorphous and crystalline GeS_x undergo irreversible transformation into unique tetragonal phase Ge nanoparticles which were found to be the active material during the reversible Li-storage. In a parallel study, $GeSe_x$ ($x = 1$ and 2) nanocrystals were also investigated as anode materials.[191] Such materials provided a reversible capacity of 400–800 $mA\,h\,g^{-1}$ after 70 cycles. In an extreme case, the sub-stoichiometric germanium sulfide thin-films,[192]

$Ge_{0.9}S_{0.1}$ and $Ge_{0.95}S_{0.05}$, showed a high rate capacity as well (900 mA h g^{-1} after 500 cycles at a rate of 20 C).

Unlike Ge-oxides, -sulfides, and -selenides, ternary germanates have several advantages including abundant elemental combinations associated with many different crystal structures, the low-cost, high conductivity,[193] and stable cycling capacity in LIBs. Consequently, the ternary germanates will be the focus of the following paragraphs.

In general, germanium compounds, such as $CuGeO_3$ adopt a conversion and alloying process during lithium cycling [Eq. (2)–(8)].[18] The crystalline structure of $CuGeO_3$ was destroyed during the first discharge, followed by the formation of GeO_2, Cu metal nanoparticles and a Li_2O buffer matrix. The newly formed GeO_2 then alloyed with Li^+ to yield Li_yGe. During the charge process, the Li_yGe alloy was first dealloyed, followed by the oxidation of Ge and Cu.

$$CuGeO_3 + xLi^+ + xe^- \rightarrow Cu^2{}_{1-x}Cu^1{}_xO_{1-x/2} + GeO_2 + \frac{x}{2}Li_2O \quad (2)$$

$$Cu^2{}_{1-x}Cu^1{}_xO_{1-x/2} + (2-x)Li^+ + (2-x)e^- \rightarrow Cu + (1-\frac{x}{2})Li_2O \quad (3)$$

$$GeO_2 + 4\,Li^+ + 4\,e^- \rightleftharpoons Ge + 2\,Li_2O \quad (4)$$

$$Ge + y\,Li^+ + y\,e^- \rightleftharpoons Li_yGe \quad (5)$$

$$Li_yGe \rightarrow Ge + yLi^+ + y\,e^- \quad (6)$$

$$Ge + 2\,Li_2O \rightleftharpoons GeO_2 + 4\,Li^+ + 4\,e^- \quad (7)$$

$$2\,Cu + Li_2O \rightleftharpoons Cu_2O + 2\,Li^+ + 2\,e^- \quad (8)$$

As early as 2009, $MGeO_3$ (M = Cu, Fe, and Co) electrodes were reported.[185] Subsequently, $CuGeO_3$ nanorods have demonstrated charge capacities of 690 mA h g^{-1} after 50 cycles at 150 mA g^{-1}.[194] A comparable result was observed in $Cu_3Ge/GeO_x/CuGeO_3$ nanowire electrodes[195] (a capacity of around 645 mA h g^{-1} at 200 mA g^{-1} after 20 cycles). In one report,[18] crystalline $CuGeO_3$ nanowires were tightly covered and anchored by graphene sheets to form a layered structure. The $CuGeO_3$ contained 37 wt% graphene and exhibited a reversible capacity of 853 mA h g^{-1} after 50 cycles at 200 mA g^{-1}.

Recently, Zn_2GeO_4 has aroused increasing interest. The charge/discharge mechanism of Zn_2GeO_4 is similar to that of $CuGeO_3$. In general, the charge/discharge mechanism of Zn_2GeO_4 can be given as follows [Eq. (9)–(16)]:[19]

Charging:

$$Zn_2GeO_4 + 8\,Li^+ + 8\,e^- \rightarrow 2\,Zn + Ge + 4\,Li_2O \quad (9)$$

$$Zn_2GeO_4 + 3\,Li^+ + 3\,e^- \rightarrow Li_3Zn_{0.5}GeO_4 + 1.5\,Zn \quad (10)$$

$$Zn + x\,Li^+ + x\,e^- \rightleftharpoons Li_xZn \qquad (0 \le x \le 1) \quad (11)$$

$$Ge + y\,Li^+ + y\,e^- \rightleftharpoons Li_yGe \qquad (0 \le y \le 4.4) \quad (12)$$

Discharging:

$$Li_yGe \rightarrow Ge + yLi^+ + y\,e^- \quad (13)$$

$$Li_xZn \rightarrow Zn + xLi^+ + x\,e^- \quad (14)$$

$$Zn + Li_2O \rightleftharpoons ZnO + 2\,Li^+ + 2\,e^- \quad (15)$$

$$Ge + 2\,Li_2O \rightleftharpoons GeO_2 + 4\,Li^+ + 4\,e^- \quad (16)$$

In 2011, Zn_2GeO_4 produced a charge capacity of 616 mA h g^{-1} at 400 mA g^{-1} at the 100th cycle.[196] Several strategies have been established to address the volume expansion of Zn_2GeO_4 electrodes during Li-cycling. Amorphous Zn_2GeO_4 particles have a stable capacity of 1250 mA h g^{-1} at the 500th cycle under a current density of 400 mA g^{-1}.[197] Recently, coaxial Zn_2GeO_4@carbon nanowires directly grown on a Cu foil (ZGO@C/Cu) were prepared by CVD.[198] The ZGO@C/Cu electrode afforded a capacity of 790 mA h g^{-1} at a large current density of 2000 mA g^{-1} over 100 cycles.

Graphene is viable matrix to support active materials in electrodes that is also able to accommodate the volume change of Zn_2GeO_4 electrodes during cycling. Hollow

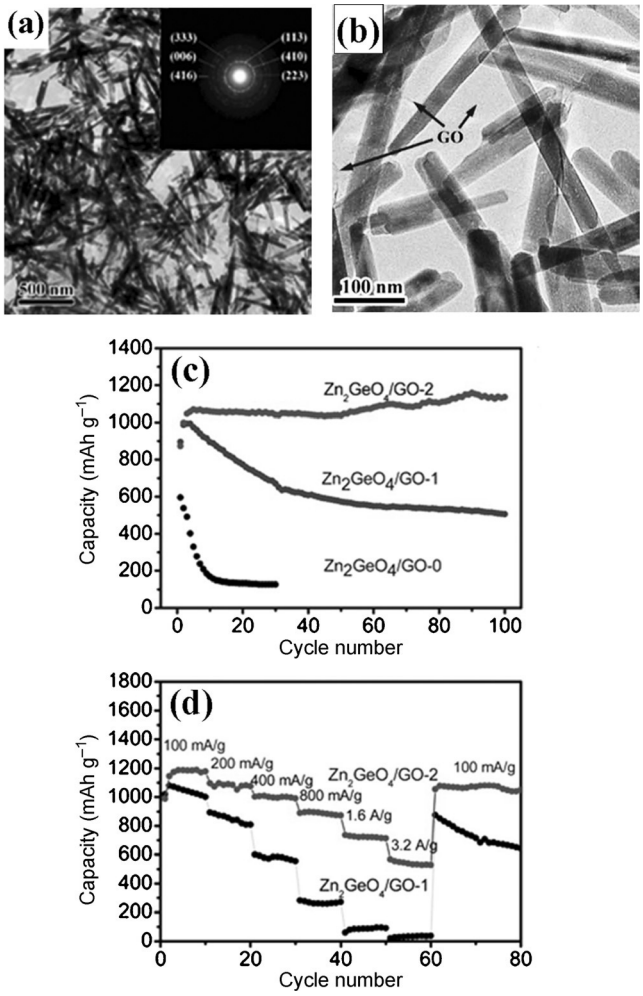

Figure 14. a),b) TEM images of the Zn_2GeO_4-GO-2 composite (inset in (a): SAED pattern). c) Cycle performance of pristine Zn_2GeO_4 (Zn_2GeO_4-GO-0) and Zn_2GeO_4-GO composites (Zn_2GeO_4-GO-1 and Zn_2GeO_4-GO-2). d) Rate performances of Zn_2GeO_4-GO-1 and Zn_2GeO_4-GO-2. Reproduced with permission from Ref. [200] Copyright 2014 The Royal Society of Chemistry.

Zn_2GeO_4/rGO hybrids demonstrated a specific capacity over 900 mA h g^{-1} at a rate of 100 mA g^{-1} (based on Zn_2GeO_4).[199] Since then, more elaborate structures have emerged. Sandwiched Zn_2GeO_4-graphene oxide nanocomposites with a specific capacity of 1150 mA h g^{-1} at 200 mA g^{-1} after 100 cycles were also reported by Zou et al. (Figure 14).[200] Another example is Zn_2GeO_4/N-doped graphene nanocomposites which demonstrated a reversible capacity of 1044 mA h g^{-1} at a current density of 100 mA g^{-1} after 100 discharge/charge cycles.[201] In another report,[19] partially crystalline Zn_2GeO_4/graphene nanocomposites containing 10.2 wt% graphene possessed a favorable cycling performance (768 mA h g^{-1} after 50 cycles at a current density of 200 mA g^{-1}) owing to the amorphous region present in partially crystalline Zn_2GeO_4 nanorods and the elastic graphene sheets.

Li-cyclabilities of other germanates are comparable to $CuGeO_3$ and Zn_2GeO_4 because they undergo almost the same alloying–dealloying mechanism. Lithium cycling of chestnut-like $Cd_2Ge_2O_6$/rGO nanocomposites produced via hydrothermal methods were surveyed and found to possess an initial capacity of 943 mA h g^{-1} and a capacity retention of 721 mA h g^{-1} after 100 cycles at a current density of 100 mA g^{-1}.[202] In situ hydrothermally produced graphene-nanosheet/$PbGeO_3$ composites delivered a discharge capacity of 607 mA h g^{-1} at 100 mA g^{-1} after 50 cycles.[203] However, the use of lead and cadmium in battery applications is less ideal for safety reasons associated with heavy metal toxicity. Recently, Fe_2GeO_4 nanoparticles (NPs)/rGO hybrids afforded a high reversible capacity of 980 mA h g^{-1} at 360 mA g^{-1} for 175 cycles (Figure 15).[204] Single-crystalline metal germanate nanowires,[205] including $SrGe_4O_9$, $BaGe_4O_9$, and Zn_2GeO_4 were successfully grown on carbon textiles via hydrothermal methods on a large scale. The germanate nanowire-carbon textiles exhibited reversible capacities in the range of 900–1000 mA h g^{-1} at 400 mA g^{-1} and good cyclability with no obvious capacity decay after 100 cycles.

In summary, germanates have been evaluated as promising anode materials owing to their stable Li-cycling performances. However, investigations into germanium compounds have concentrated on $CuGeO_3$ and Zn_2GeO_4 largely because of their facile synthesis routes. Owing to the unique crystal structure of germanium compounds, there are difficulties in producing some germanates, such as $MgGeO_3$ and $FeGeO_3$, in a simple, low-cost process. More practical routes need to be explored and developed to expand the accessible germanate family and thereby create more potential Li-storage materials.

3. Anode Materials for Sodium-Ion Batteries (SIBs)

As mentioned above, potential next-generation energy storage devices include flow batteries,[1] vanadium flow batteries,[2] Li–S batteries, sodium-ion batteries, Li–O_2 batter-

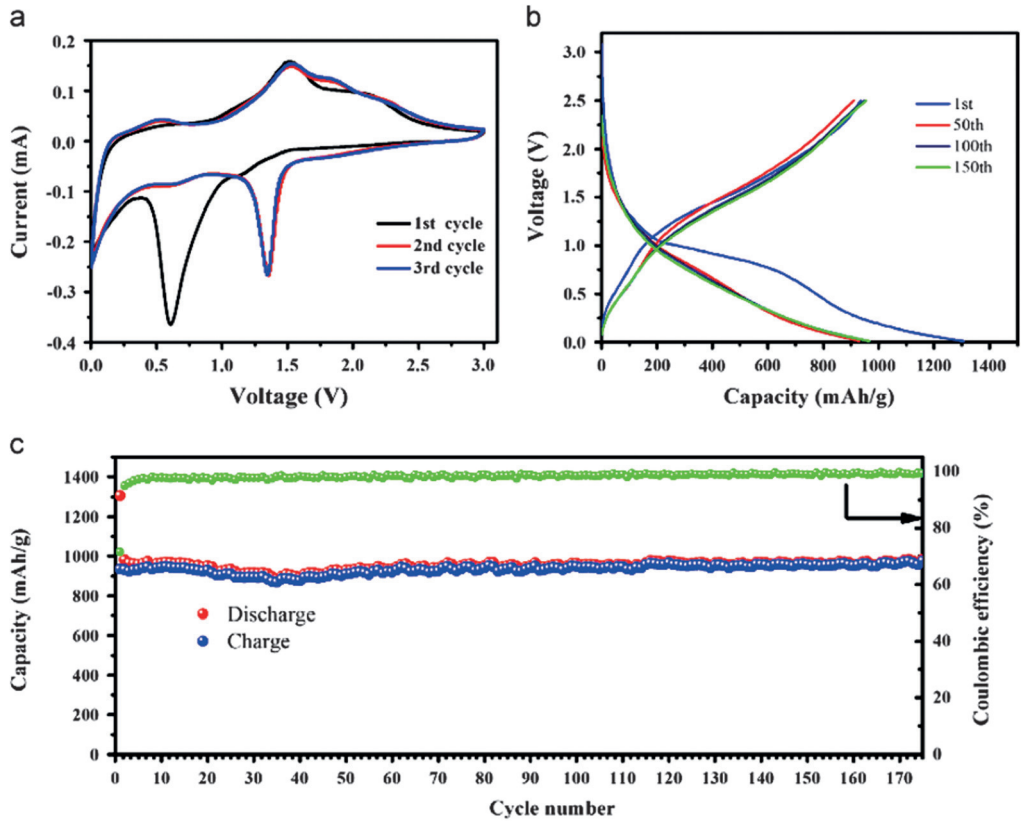

Figure 15. Electrochemical performance of the Fe_2GeO_4 NPs/RGO anode. a) Cyclic voltammetry (CV) profiles for the first three cycles. b) Voltage profiles of the electrode at a current density of 360 mA g^{-1}. c) Cycling performances of the electrodes at a current density of 360 mA g^{-1}. Reproduced with permission from Ref. [204] Copyright 2014 Elsevier.

ies,[3,4b] and aluminum-ion batteries.[206] In the next two Sections, attention will be given to solid-state lithium batteries,[207,208] metal–air batteries,[86,209] and sodium-ion batteries[210] in which Ge-based materials have recently gained popularity.

SIBs are a rising next-generation energy-storage technology that has even seen small-scale commercialization in recent years.[102] Ge-based materials may also find themselves in a suitable position to serve as a promising anode material during sodium-ion cycling in an analogous fashion to lithium ions.

In thin-film electrodes, germanium electrochemically reacts with Na to form Na–Ge alloys at potentials ranging from 0.15 V to 0.6 V versus Na/Na^+, which can be expected to deliver a reversible capacity approximately 350 $mA\,h\,g^{-1}$.[210] Subsequently, various thin-film morphologies have been investigated for achieving different Na-storage capabilities.[211] Nano-columnar films produced via evaporative deposition maintained a reversible capacity of 430 $mA\,h\,g^{-1}$ with 88% capacity retention after 100 cycles at 0.2 C. In comparison, dense films began to deteriorate after 15 cycles and showed overall poor electrochemical performance.[212] Modeling of diffusion in the sodium–germanium system predicts that sodium diffusion in the near-surface layers of the material is considerably faster than in the bulk. This suggests that high surface area morphologies are more amenable to fast charging and discharging. Similarly, germanium nanowires (GeNWs) and Ge thin films maintained analogous electrochemical responses with reversible (de-sodiation) capacities of 346 and 418 $mA\,h\,g^{-1}$ at 0.15 C (1 C = 369 $mA\,g^{-1}$, Na/Ge 1:1) for 50 cycles.[212]

In addition to pure germanium-based morphologies for sodium-ion storage, bimetallic alloys have also been investigated for this purpose. While the stability of the Ge-Sn alloys is greatly increased with an increasing amount of Ge, the specific reversible capacity of the alloy decreases with increasing germanium content owing to the lower reversible capacity of germanium (Figure 16).[213] 3D Si/Ge nanorod array anodes buffered by a TiN/Ti interlayer for SIBs were recently reported by Yue et al.[168] This anode material presented an improved cycle performance of 400 $mA\,h\,g^{-1}$ up to 200 cycles and specific capacities of 390 $mA\,h\,g^{-1}$ at 400 $mA\,g^{-1}$ and 230 $mA\,h\,g^{-1}$ at 4000 $mA\,g^{-1}$.

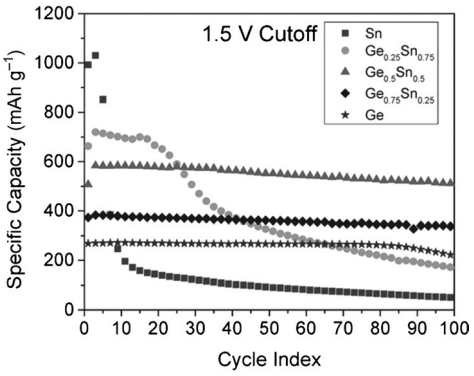

Figure 16. Stability of Sn–Ge alloy films cycled at C/2 between a lower cutoff voltage of 5 mV and an upper cutoff voltage of 1.5 V. Reproduced with permission from Ref. [213] Copyright 2014 The American Chemical Society.

The trend continues with similar investigations into even more complex three-component anode materials for SIBs. Specifically, ternary Sn–Ge–Sb thin film alloys have the potential to act as sodium ion battery anode materials.[214] $Sn_{33}Ge_{33}Sb_{33}$, $Sn_{50}Ge_{25}Sb_{25}$, $Sn_{60}Ge_{20}Sb_{20}$, and $Sn_{50}Ge_{50}$ demonstrate promising electrochemical properties. Among them, $Sn_{50}Ge_{25}Sb_{25}$ alloys afforded an initial reversible specific capacity of 833 $mA\,h\,g^{-1}$ (at 85 $mA\,g^{-1}$), which is the highest reversible capacity reported for a Sn-based SIB anode to date, and 662 $mA\,h\,g^{-1}$ after 50 cycles. The corresponding solid-state electrolyte has been under investigation.[215]

It should be noted that sodium-ion batteries are in their infancy when compared to established LIB technology. Whether or not SIBs will be a displacing or parallel technology remains to be seen. Despite this, the significantly lower cost and greater abundance of sodium-based salts for use in energy-storage in batteries will likely continue to drive development in this field. The possibility that Ge-based materials will be used in SIB-based energy-storage devices is also uncertain. However, the multitude of single, binary, and ternary materials suggests the likelihood of their application in this emerging technology in some form.

4. Ge-Based Solid Electrolytes and Others

A major concern in the development of rechargeable batteries is safety. Conventional batteries usually use liquid electrolytes, which contain highly volatile and flammable organic solvents and may lead to safety hazards, especially when being coupled with a Li metal anode. Compared with conventional liquid/gel-based batteries, all-solid-state lithium batteries are leak proof, mechanically robust, and can be used over a wider range of temperatures. Bulk-type solid-state cells composed of electrode and electrolyte powders are advantageous in achieving large energy densities and higher safety.[216,217]

Solid electrolytes that are lithium-ion conducting are a decisive component of all-solid-state batteries, and could provide high-energy-density batteries with distinctive safety features over traditional liquid electrolytes.[218] As a new Li-ion solid electrolyte, $Li_{3.334}Ge_{0.334}As_{0.666}S_4$, demonstrates a high ionic conductivity of 1.12 $mS\,cm^{-1}$ at 27 °C. Local Li^+ hopping in this material was accompanied by a low activation energy E_a of 0.17 eV. Another fast ion conductor $Li_{1-x}Al_xGe_{2-x}(PO_4)_3$ (LAGP)[219,220] has demonstrated a higher bulk conductivity (10^{-4} $S\,cm^{-1}$ at room temperature).[219] In a very recent report,[221] a Li–air battery with SWCNTs/LAGP showed improved cycling performance with a reversible capacity of 1000 $mA\,h\,g^{-1}$ at a current density of 200 $mA\,g^{-1}$. The lithium–oxygen battery using $Li_{1.575}Al_{0.5}Ge_{1.5}(PO_4)_3$ solid electrolyte was examined in pure oxygen atmosphere from room temperature to 120 °C. The cell works at room temperature and the first full discharge capacity of 1420 $mA\,h\,g^{-1}$ at 10 $mA\,g^{-1}$ (based on the mass of carbon material in the air electrode) was obtained.[222] The all-solid-state $Li/LiFePO_4$ cell assembled with LAGP/poly(ethylene oxide) hybrid solid electrolyte

delivered an initial discharge capacity of 138 mA h g^{-1} and exhibited good cycling stability at 55 °C.[223] In 2013, TDK Corporation filed a patent for an inorganic all-solid-state secondary battery for personal computers containing a solid electrolyte layer, positive electrode layer, and negative electrode layer which contains crystallized lithium–aluminum–germanium–phosphate (LAGP) glass.[224]

The inorganic composition that Kamaya et al. report, $Li_{10}GeP_2S_{12}$, showed the highest lithium-ion conductivity ever measured for a solid of 12 mS cm^{-1} at 300 K. The material has a three-dimensional structure that consists of $(Ge_{0.5}P_{0.5})S_4$ tetrahedra, PS_4 tetrahedra, LiS_4 tetrahedra, and LiS_6 octahedra (Figure 17).[216,225] The related first-principles calculations[226] suggest that $Li_{10}GeP_2S_{12}$ (LGPS) is capable of providing the highest Li^+ conductivity to date in the

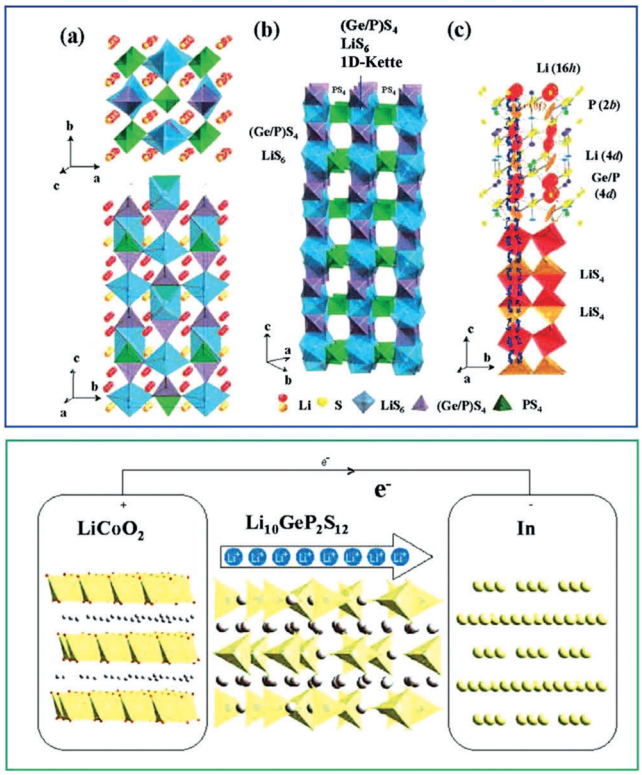

Figure 17. Top panels: Crystal structure of $Li_{10}GeP_2S_{12}$. a) The framework structure and lithium ions that participate in ionic conduction. b) Framework structure of $Li_{10}GeP_2S_{12}$. One-dimensional (1D) chains formed by LiS_6 octahedra and $(Ge_{0.5}P_{0.5})S_4$ tetrahedra, which are connected by a common edge. These chains are connected by a common corner with PS_4 tetrahedra. c) Conduction pathways of lithium ions. Zigzag conduction pathways along the *c* axis are indicated. Lithium ions in the LiS_4 tetrahedra (16*h* site) and LiS_4 tetrahedra (8*f* site) participate in ionic conduction. Thermal ellipsoids are set at 30% probability. The anisotropic character of the thermal vibration of lithium ions in three tetrahedral sites gives rise to 1D conduction pathways. Reproduced with permission from Ref. [225] Copyright 2011 Nature. Bottom panels: Schematic view of the all-solid-state lithium-ion battery reported by Kamaya and co-workers. During charging, lithium ions (gray) travel with high mobility from the positive $LiCoO_2$ electrode to the negative indium electrode via partially occupied LiS_4 tetrahedra and interstitial positions in the new superionic conductor $Li_{10}GeP_2S_{12}$. Reproduced with permission from Ref. [216] Copyright 2011 Nature.

$Li_{10\pm1}MP_2X_{12}$ family of conductors (M = Ge, Si, Sn, Al, or P; X = O, S, or Se). Developments have been observed in several solid-state lithium batteries containing $LiNi_{0.8}Co_{0.15}Al_{0.05}O_2$ (NCA) cathodes with improved performance (72.3 mA h g^{-1} at 1 C) and cycling stability (capacity retention of 87.1% after 30 cycles at 0.1 C) for $Li_{10}GeP_2S_{12}$ based batteries.[227] Similarly, all-solid electrolytes for sodium transport have also been under investigation.[215] The sodium salt, $Na_{1+x}Y_yGa_{x-y}Ge_{2-x}(PO_4)_3$ (NYGGP) has been considered as a solid electrolyte for sodium-ion batteries due to its high ionic conductivity of 1.40×10^{-3} S cm^{-1} at 300 °C (1.15×10^{-5} S cm^{-1} at room temperature) and low activation energy around 20.5 kJ mol^{-1} at 300 °C.[215] Despite promising improvements in solid electrolytes, the conductivity is still relatively low and it is in no position to compete with commercial liquid electrolytes such as $LiPF_6$ which has a conductivity of approximately 10 mS cm^{-1}. The all-solid-state LIB still has a long way to go before commercialization is possible.

Metal–air batteries are another attractive energy-storage and conversion system owing to their high energy and power densities, safer chemistries, and economic viability. In 2013, Ocon and co-workers[228] first reported a high power density Ge-air energy conversion cell using germanium with ordered hierarchical porous structures as an anode. In subsequent work, the excellent doping-dependent discharge kinetics of p-type Ge anodes in a semiconductor–air cell employing gelled KOH as the electrolyte were demonstrated.[86] One semiconductor-air battery showed an unprecedented full discharge capacity of 1303 mA h g^{-1} (based on Ge with 88% anode utilization efficiency). This is one of the highest values reported among semiconductor–air cells to date and is at least twice as large as commercial Zn–air and Al–air cells.

Recently, magnesium-ion batteries have also been considered as a substitute for lithium-ion batteries because of the high volumetric capacity (3832 mA h cm^{-3}), improved safety (nondendritic), and abundance of Mg metal.[228] In an interesting study,[229] Sn and Ge were incorporated into Mg batteries because of their small lattice expansions (ca. 120% and ca. 178%, respectively) and low diffusion barriers (ca. 0.50 and ca. 0.70 eV, respectively). Mg–Mg interactions at different stages of charging significantly decreased the diffusion barrier compared to single-atom diffusion by up to 0.55 eV.[229]

As previously mentioned, the application of Ge-based materials in next-generation energy-storage devices is only just emerging. However, there is potential for future development and device improvement. In particular the solid electrolyte used in all-solid-state batteries is promising as a result of the high conductivity of germanate.

5. Conclusions and Outlook

Today, germanium is mainly mined from sphalerite, and ranks fiftieth in abundance in the Earth's crust. The largest use of this material used to be in applications involving solid-state electronics, in the form of germanium transistors. However, as of 2007, the major end-uses for germanium are

in fiber-optic systems (35%) and infrared optics (30%) with only 15% retained for electronics and solar electric applications. In 2014, the consumption of germanium in USA for fiber-optic systems increased compared with that in 2013 but its use in infrared optics declined over the same period. The estimated value of germanium metal consumed in 2014 was about $67 million.[39]

Recently, two new major uses of germanium in the field of energy storage and conversion have been solar panels and battery materials. Electrode materials and electrolytes largely dictate the cycle life and energy-storage capability of resulting battery devices. With the development of high-power electronic devices, there is a demand for new electrode materials that can support large current cycling over many cycles. Among anode materials, Ge-based materials have shown promise in the crucial components of high-energy batteries, including LIBs and SIBs, owing to their high carrier mobility (electronic and hole mobility), large theoretical capacity, and excellent mechanical strength. The large number and variety of research efforts in this area are very encouraging and will undoubtedly drive the progress of energy-storage and conversion devices.

In this Review, a brief summary on the current state-of-the-art progress and challenges of Ge-based materials for next-generation battery has been presented. From the viewpoint of technology, both pure germanium and Ge-based alloys possess several interesting properties motivating the use of germanium in diverse ways. Firstly, it is very easy to achieve porous structures for Ge and Ge alloys because of the unique porous structure of the GeO_2 template. The porous nature of these materials enables the accommodation of volume expansion during Li-cycling either through adsorbed amorphous carbon, such as carbon black, the porous nanostructure of the materials themselves, or a phase transformation between crystalline and amorphous types. Secondly, the high conductivity and fast Li-mobility of Ge-based materials enables improved cycling performance. Lastly, the use of graphene (anchored, wrapped, sandwich-like, or encapsulated) or amorphous carbon has helped to alleviate volume changes during cycling. This reduces the degree of electrode destruction and improves cycling stability. Consequently, Ge-based hybrid materials have achieved notable success for use in both the anode of LIBs (or SIBs) and electrolyte of solid-state batteries.

As to anodes, a number of reports have provided a framework for germanium-based material categories. These categories cover porous pure germanium, germanium–carbon hybrids (graphene, amorphous carbon, CNT, or CNF etc.) and Ge-based alloys. However, there are several challenges that need to be dealt with in future development:

a) Various structures and morphologies need to be designed to lay a foundation for understanding the influence of the structure and material composition on the lithium-storage mechanism. That is, a larger family of nanostructured Ge-based anode materials needs to be developed with further improvement in the electrochemical performance of the resultant batteries.
b) Despite porous germanium electrodes exhibiting remarkable Li(Na)-cycling performances, a greater understanding of the origin of the Li(Na)-cycling capability, particularly at large current densities, is of importance in understanding the relationship between structure and performance. In addition, the influence of finite size effects from Ge nanoparticles or GE based alloy nanocomposites on Li-storage properties needs to be further understood.
c) To meet industrial applications, easily controlled and cost-effective synthesis approaches are required. CVD is a commonly used method to produce various Ge-based materials with versatile microstructures. Facile wet chemical reactions have also proven advantageous owing to their high yield and simplicity. Further research into employing these industry-standard techniques is required.
d) The conductivity of Ge-based solid electrolytes is currently too low to commercialize for Li-ion battery applications for typical uses at ambient temperature. All-solid-state batteries using Ge-based solid electrolytes may find an opportunity in energy storage at power stations and smart grids. Such environments are not sensitive to the volume of the battery packages. The focus is on storing as much energy as possible. Portable electronics are less amenable to all-solid-state batteries because of the size and weight requirements imposed.

Breaking out of their almost exclusive use in the semiconductor industry, Ge-based materials have slowly and quietly established themselves as promising candidates for vital components of high-energy-storage devices. There is much evidence, as detailed herein, to suggest that Ge-based materials will play an increasingly active role in the next generation of energy storage devices.

Acknowledgements

S.P.W. gratefully acknowledges the financial support from the Department of Science and Technology of Guangdong (No. 2014B010123001, No. 2015B090901030, No. 2016B050502004), Department of Science and Technology of Guangzhou (No. 2016201604030013) and Foshan Shunde CG Electronic Industry Co., Ltd. This work is also supported by Georgia Institute of Technology (Z.L.).

How to cite: *Angew. Chem. Int. Ed.* **2016**, *55*, 7898–7922
Angew. Chem. **2016**, *128*, 8028–8054

[1] B. Huskinson, M. P. Marshak, C. Suh, S. Er, M. R. Gerhardt, C. J. Galvin, X. Chen, A. Aspuru-Guzik, R. G. Gordon, M. J. Aziz, *Nature* **2014**, *505*, 195–198.
[2] R. F. Service, *Science* **2014**, *344*, 352–354.
[3] M. M. Ottakam Thotiyl, S. A. Freunberger, Z. Peng, Y. Chen, Z. Liu, P. G. Bruce, *Nat. Mater.* **2013**, *12*, 1050–1056.
[4] a) P. G. Bruce, S. A. Freunberger, L. J. Hardwick, J. M. Tarascon, *Nat. Mater.* **2012**, *11*, 19–29; b) Z. Q. Peng, S. A. Freunberger, Y. H. Chen, P. G. Bruce, *Science* **2012**, *337*, 563–566.
[5] I. Gur, K. Sawyer, R. Prasher, *Science* **2012**, *335*, 1454–1455.
[6] B. Dunn, H. Kamath, J. M. Tarascon, *Science* **2011**, *334*, 928–935.

[7] P. Hartmann, C. L. Bender, M. Vračar, A. K. Dürr, A. Garsuch, J. Janek, P. Adelhelm, *Nat. Mater.* **2013**, *12*, 228 – 232.
[8] R. E. Doe, R. Han, J. Hwang, A. J. Gmitter, I. Shterenberg, H. D. Yoo, N. Pour, D. Aurbach, *Chem. Commun.* **2014**, *50*, 243 – 245.
[9] US Advanced Battery Consortium USABC Goals for Advanced Batteries for EVs (2006). Available at: http://uscar.org/commands/files_download.php?files_id = 27.
[10] D. Larcher, J. M. Tarascon, *Nat. Chem.* **2015**, *7*, 19 – 29.
[11] R. Van Noorden, *Nature* **2014**, *507*, 26 – 28.
[12] Q. Wang, Z. H. Wen, J. H. Li, *Adv. Funct. Mater.* **2006**, *16*, 2141 – 2146.
[13] L. F. Cui, Y. Yang, C. Hsu, Y. Cui, *Nano Lett.* **2009**, *9*, 3370 – 3374.
[14] C. K. Chan, X. F. Zhang, Y. Cui, *Nano Lett.* **2008**, *8*, 307 – 309.
[15] G. Jo, I. Choi, H. Ahn, M. J. Park, *Chem. Commun.* **2012**, *48*, 3987 – 3989.
[16] X. W. Lou, Y. Wang, C. Yuan, J. Y. Lee, L. A. Archer, *Adv. Mater.* **2006**, *18*, 2325 – 2329.
[17] G. Zhou, D. Wang, F. Li, L. Zhang, N. Li, Z. Wu, L. Wen, G. Q. Lu, H. Cheng, *Chem. Mater.* **2010**, *22*, 5306 – 5313.
[18] S. Wu, R. Wang, Z. Wang, Z. Lin, *Nanoscale* **2014**, *6*, 8350 – 8358.
[19] R. Wang, S. Wu, Y. Lv, Z. Lin, *Langmuir* **2014**, *30*, 8215 – 8220.
[20] Y. Jing, E. O. Ortiz-Quiles, C. R. Cabrera, Z. F. Chen, Z. Zhou, *Electrochim. Acta* **2014**, *147*, 392 – 400.
[21] L. David, R. Bhandavat, G. Singh, *ACS Nano* **2014**, *8*, 1759 – 1770.
[22] S. Y. Liu, X. Lu, J. Xie, G. S. Cao, T. J. Zhu, X. B. Zhao, *ACS Appl. Mater. Interfaces* **2013**, *5*, 1588 – 1595.
[23] C. D. Wang, Y. S. Chui, Y. Li, X. F. Chen, W. J. Zhang, *Appl. Phys. Lett.* **2013**, *103*, 253903.
[24] Y. Xu, X. S. Zhu, X. S. Zhou, X. Liu, Y. X. Liu, Z. H. Dai, J. C. Bao, *J. Phys. Chem. C* **2014**, *118*, 28502 – 28508.
[25] H. A. Tahini, A. Chroneos, S. C. Middleburgh, U. Schwingenschlogl, R. W. Grimes, *J. Mater. Chem. A* **2015**, *3*, 3832 – 3838.
[26] B. Farbod, K. Cui, W. P. Kalisvaart, M. Kupsta, B. Zahiri, A. Kohandehghan, E. M. Lotfabad, Z. Li, E. J. Luber, D. Mitlin, *ACS Nano* **2014**, *8*, 4415 – 4429.
[27] Y. D. Zhang, J. Xie, T. J. Zhu, G. S. Cao, X. B. Zhao, S. C. Zhang, *J. Power Sources* **2014**, *247*, 204 – 212.
[28] J. Shin, K. Park, W. H. Ryu, J. W. Jung, I. D. Kim, *Nanoscale* **2014**, *6*, 12718 – 12726.
[29] C. K. Chan, H. Peng, G. Liu, K. McIlwrath, X. F. Zhang, R. A. Huggins, Y. Cui, *Nat. Nanotechnol.* **2008**, *3*, 31 – 35.
[30] http://www.btrchina.com/product/index123.html#comment.
[31] http://www.shanshantech.com/Productsinfo.aspx?ProductsID = 18&CateId = 86.
[32] a) H. Wu, Y. Cui, *Nano Today* **2012**, *7*, 414 – 429; b) H. Kim, E. J. Lee, Y. K. Sun, *Mater. Today* **2014**, *17*, 285 – 297; c) J. Cho, *J. Mater. Chem.* **2010**, *20*, 4009 – 4014.
[33] A. Moguš-Milanković, K. Sklepić, H. Blažanović, P. Mošner, M. Vorokhta, L. Koudelka, *J. Power Sources* **2013**, *242*, 91 – 98.
[34] H. G. Na, D. S. Kwak, Y. J. Kwon, H. Y. Cho, H. W. Kim, *J. Ceram. Process. Res.* **2013**, *14*, 391 – 395.
[35] D. Back, J. Lee, *J. Nanosci. Nanotechnol.* **2014**, *14*, 8999 – 9004.
[36] M. Mošner, S. Wippermann, B. Somogyi, A. Gali, D. Rocca, G. Galli, G. T. Zimanyi, *J. Mater. Chem. A* **2014**, *2*, 9820 – 9827.
[37] A. Jain, E. Kawasako, H. Miyaoka, T. Ma, S. Isobe, T. Ichikawa, Y. Kojima, *J. Phys. Chem. C* **2013**, *117*, 5650 – 5657.
[38] F. Lévy, I. Sheikin, B. Grenier, A. D. Huxley, *Science* **2005**, *309*, 1343 – 1346.
[39] U. S. G. Survey, U.S. Geological Survey, Mineral Commodity Summaries, Januar **2015**.
[40] N. G. Rudawski, B. R. Yates, M. R. Holzworth, K. S. Jones, R. G. Elliman, A. A. Volinsky, *J. Power Sources* **2013**, *223*, 336 – 340.
[41] X. L. Wu, Y. G. Guo, L. J. Wan, *Chem. Asian J.* **2013**, *8*, 1948 – 1958.
[42] C. O'Regan, S. Biswas, N. Petkov, J. D. Holmes, *J. Mater. Chem. C* **2014**, *2*, 14 – 33.
[43] Y. Liu, S. L. Zhang, T. Zhu, *ChemElectroChem* **2014**, *1*, 706 – 713.
[44] L. Z. Pei, Z. Y. Cai, *Recent Pat. Nanotechnol.* **2012**, *6*, 44 – 59.
[45] D. D. Vaughn II, R. E. Schaak, *Chem. Soc. Rev.* **2013**, *42*, 2861 – 2879.
[46] Y. H. Chen, Y. Z. Li, G. Z. Wang, Q. Di, Y. S. Shen, N. Sun, Z. Y. Tang, *J. Wuhan Univ. Technol. Mater. Sci. Ed.* **2012**, *27*, 212 – 216.
[47] M. V. Reddy, G. V. S. Rao, B. V. R. Chowdari, *Chem. Rev.* **2013**, *113*, 5364 – 5457.
[48] Y. Oumellal, A. Rougier, G. A. Nazri, J. M. Tarascon, L. Aymard, *Nat. Mater.* **2008**, *7*, 916 – 921.
[49] C.-Y. Chou, H. Kim, G. S. Hwang, *J. Phys. Chem. C* **2011**, *115*, 20018 – 20026.
[50] L. Y. Ma, J. S. Gu, E. Fahrenkrug, S. Maldonado, *J. Electrochem. Soc.* **2014**, *161*, D3044 – D3050.
[51] B. R. Long, J. L. Goldman, R. G. Nuzzo, A. A. Gewirth, *J. Solid State Electrochem.* **2013**, *17*, 3015 – 3020.
[52] B. Farbod, K. Cui, M. Kupsta, W. P. Kalisvaart, E. Memarzadeh, A. Kohandehghan, B. Zahiri, D. Mitlin, *J. Mater. Chem. A* **2014**, *2*, 16770 – 16785.
[53] X. F. Liu, C. Giordano, M. Antonietti, *J. Mater. Chem.* **2012**, *22*, 5454 – 5459.
[54] C. H. Kim, H. S. Im, Y. J. Cho, C. S. Jung, D. M. Jang, Y. Myung, H. S. Kim, S. H. Back, Y. R. Lim, C. W. Lee, J. Park, M. S. Song, W. I. Cho, *J. Phys. Chem. C* **2012**, *116*, 26190 – 26196.
[55] S. Fang, L. F. Shen, P. Nie, G. Y. Xu, J. Wang, X. G. Zhang, *J. Mater. Sci.* **2014**, *49*, 2279 – 2285.
[56] T. Song, Y. Jeon, M. Samal, H. Han, H. Park, J. Ha, D. K. Yi, J. M. Choi, H. Chang, Y. M. Choi, U. Paik, *Energy Environ. Sci.* **2012**, *5*, 9028 – 9033.
[57] A. Lahiri, A. Willert, S. Z. El Abedin, F. Endres, *Electrochim. Acta* **2014**, *121*, 154 – 158.
[58] Z. G. Wang, Q. L. Su, H. Q. Deng, W. D. He, J. H. Lin, Y. Q. Fu, *J. Mater. Chem. A* **2014**, *2*, 13976 – 13982.
[59] N. K. Mahenderkar, Y. C. Liu, J. A. Koza, J. A. Switzer, *ACS Nano* **2014**, *8*, 9524 – 9530.
[60] X. H. Liu, S. Huang, S. T. Picraux, J. Li, T. Zhu, J. Y. Huang, *Nano Lett.* **2011**, *11*, 3991 – 3997.
[61] J. De Haeck, T. B. Tai, S. Bhattacharyya, H. T. Le, E. Janssens, M. T. Nguyen, P. Lievens, *Phys. Chem. Chem. Phys.* **2013**, *15*, 5151 – 5162.
[62] C. Y. Chou, G. S. Hwang, *J. Power Sources* **2014**, *263*, 252 – 258.
[63] L. Y. Lim, N. Liu, Y. Cui, M. F. Toney, *Chem. Mater.* **2014**, *26*, 3739 – 3746.
[64] M. Zeilinger, T. F. Fässler, *Dalton Trans.* **2014**, *43*, 14959 – 14970.
[65] A. J. Morris, C. P. Grey, C. J. Pickard, *Phys. Rev. B* **2014**, *90*, 054111.
[66] L. Baggetto, E. J. M. Hensen, P. H. L. Notten, *Electrochim. Acta* **2010**, *55*, 7074 – 7079.
[67] W. Tang, Y. P. Liu, C. X. Peng, M. Y. Hu, X. C. Deng, M. Lin, J. Z. Hu, K. P. Loh, *J. Am. Chem. Soc.* **2015**, *137*, 2600 – 2607.
[68] K. E. Silberstein, M. A. Lowe, B. Richards, J. Gao, T. Hanrath, H. D. Abruna, *Langmuir* **2015**, *31*, 2028 – 2035.
[69] H. Jung, P. K. Allan, Y. Y. Hu, O. J. Borkiewicz, X. L. Wang, W. Q. Han, L. S. Du, C. J. Pickard, P. J. Chupas, K. W. Chapman, A. J. Morris, C. P. Grey, *Chem. Mater.* **2015**, *27*, 1031 – 1041.
[70] M. Gu, H. Yang, D. E. Perea, J. G. Zhang, S. L. Zhang, C. M. Wang, *Nano Lett.* **2014**, *14*, 4622 – 4627.
[71] W. T. Liang, H. Yang, F. F. Fan, Y. Liu, X. H. Liu, J. Y. Huang, T. Zhu, S. L. Zhang, *ACS Nano* **2013**, *7*, 3427 – 3433.

[72] J. N. Weker, N. Liu, S. Misra, J. C. Andrews, Y. Cui, M. F. Toney, *Energy Environ. Sci.* **2014**, *7*, 2771 – 2777.
[73] F. S. Ke, K. Mishra, L. Jamison, X. X. Peng, S. G. Ma, L. Huang, S. G. Sun, X. D. Zhou, *Chem. Commun.* **2014**, *50*, 3713 – 3715.
[74] C. J. Zhang, Z. Lin, Z. Z. Yang, D. D. Xiao, P. Hu, H. X. Xu, Y. L. Duan, S. P. Pang, L. Gu, G. L. Cui, *Chem. Mater.* **2015**, *27*, 2189 – 2194.
[75] M. H. Park, K. Kim, J. Kim, J. Cho, *Adv. Mater.* **2010**, *22*, 415 – 418.
[76] H. P. Jia, R. Kloepsch, X. He, J. P. Badillo, P. F. Gao, O. Fromm, T. Placke, M. Winter, *Chem. Mater.* **2014**, *26*, 5683 – 5688.
[77] A. M. Chockla, K. C. Klavetter, C. B. Mullins, B. A. Korgel, *ACS Appl. Mater. Interfaces* **2012**, *4*, 4658 – 4664.
[78] C. K. Chan, X. F. Zhang, Y. Cui, *Nano Lett.* **2008**, *8*, 307 – 309.
[79] J. S. Gu, S. M. Collins, A. I. Carim, X. G. Hao, B. M. Bartlett, S. Maldonado, *Nano Lett.* **2012**, *12*, 4617 – 4623.
[80] N. G. Rudawski, B. L. Darby, B. R. Yates, K. S. Jones, R. G. Elliman, A. A. Volinsky, *Appl. Phys. Lett.* **2012**, *100*, 083111.
[81] Y. D. Ko, J. G. Kang, G. H. Lee, J. G. Park, K. S. Park, Y. H. Jin, D. W. Kim, *Nanoscale* **2011**, *3*, 3371 – 3375.
[82] T. Kennedy, E. Mullane, H. Geaney, M. Osiak, C. O'Dwyer, K. M. Ryan, *Nano Lett.* **2014**, *14*, 716 – 723.
[83] X. Liu, J. P. Zhao, Y. W. Zhang, X. K. An, Y. B. Ding, Y. Zhang, Y. Li, F. Endres, *Z. Phys. Chem. Int. J. Res. Phys. Chem. & Chem. Phys.* **2013**, *227*, 1731 – 1739.
[84] D. S. Wang, Z. B. Yang, F. Li, D. Q. Liu, X. H. Wang, H. Q. Yan, D. Y. He, *Mater. Lett.* **2011**, *65*, 1542 – 1544.
[85] S. T. Ling, Z. H. Cui, G. W. She, X. X. Guo, L. X. Mu, W. S. Shi, *J. Nanosci. Nanotechnol.* **2012**, *12*, 213 – 217.
[86] J. D. Ocon, J. W. Kim, G. H. A. Abrenica, J. K. Lee, J. Lee, *Phys. Chem. Chem. Phys.* **2014**, *16*, 22487 – 22494.
[87] X. S. Liu, J. Hao, X. X. Liu, C. X. Chi, N. Li, F. Endres, Y. Zhang, Y. Li, J. P. Zhao, *Chem. Commun.* **2015**, *51*, 2064 – 2067.
[88] E. Mullane, T. Kennedy, H. Geaney, K. M. Ryan, *ACS Appl. Mater. Interfaces* **2014**, *6*, 18800 – 18807.
[89] M. H. Park, Y. Cho, K. Kim, J. Kim, M. L. Liu, J. Cho, *Angew. Chem. Int. Ed.* **2011**, *50*, 9647 – 9650; *Angew. Chem.* **2011**, *123*, 9821 – 9824.
[90] Z. B. Yang, S. Bai, H. W. Yue, X. W. Li, D. Q. Liu, S. M. Lin, F. Li, D. Y. He, *Mater. Lett.* **2014**, *136*, 107 – 110.
[91] S. Fang, L. F. Shen, P. Nie, G. Y. Xu, L. Yang, H. Zheng, X. G. Zhang, *Part. Part. Syst. Charact.* **2015**, *32*, 364 – 372.
[92] X. W. Li, Z. B. Yang, Y. J. Fu, L. Qiao, D. Li, H. W. Yue, D. Y. He, *ACS Nano* **2015**, *9*, 1858 – 1867.
[93] M. D. Stoller, S. Park, Y. Zhu, J. An, R. S. Ruoff, *Nano Lett.* **2008**, *8*, 3498 – 3502.
[94] K. S. Novoselov, A. K. Geim, S. V. Morozov, D. Jiang, Y. Zhang, S. V. Dubonos, I. V. Grigorieva, A. A. Firsov, *Science* **2004**, *306*, 666 – 669.
[95] A. A. Balandin, *Nat. Mater.* **2011**, *10*, 569 – 581.
[96] P. Lian, X. Zhu, S. Liang, Z. Li, W. Yang, H. Wang, *Electrochim. Acta* **2010**, *55*, 3909 – 3914.
[97] S. Q. Chen, P. Chen, Y. Wang, *Nanoscale* **2011**, *3*, 4323 – 4329.
[98] Y. L. Zou, X. Y. Zhou, J. Yang, *RSC Adv.* **2014**, *4*, 25552 – 25555.
[99] O. Vargas, A. Caballero, J. Morales, E. Rodriguez-Castellon, *ACS Appl. Mater. Interfaces* **2014**, *6*, 3290 – 3298.
[100] H.-J. Peng, J.-Q. Huang, M.-Q. Zhao, Q. Zhang, X.-B. Cheng, X.-Y. Liu, W.-Z. Qian, F. Wei, *Adv. Funct. Mater.* **2014**, *24*, 2772 – 2781.
[101] S. Wu, R. Xu, M. Lu, R. Ge, J. Iocozzia, C. Han, B. Jiang, Z. Lin, *Adv. Energy Mater.* **2015**, *5*, 1500400.
[102] S. Wu, R. Ge, M. Lu, R. Xu, Z. Zhang, *Nano Energy* **2015**, *15*, 379 – 405.
[103] H. Song, H. Cui, C. Wang, *ACS Appl. Mater. Interfaces* **2014**, *6*, 13765 – 13769.
[104] R. Raccichini, A. Varzi, S. Passerini, B. Scrosati, *Nat. Mater.* **2015**, *14*, 271 – 279.
[105] J. S. Cheng, J. Du, *CrystEngComm* **2012**, *14*, 397 – 400.
[106] X. W. Zhong, J. Q. Wang, W. H. Li, X. W. Liu, Z. Z. Yang, L. Gu, Y. Yu, *RSC Adv.* **2014**, *4*, 58184 – 58189.
[107] J. W. Qin, X. Wang, M. H. Cao, C. W. Hu, *Chem. Eur. J.* **2014**, *20*, 9675 – 9682.
[108] H. B. Yin, J. M. Luo, P. H. Yang, P. H. Yin, *Nanoscale Res. Lett.* **2013**, *8*, 422.
[109] Y. Xiao, M. H. Cao, *ACS Appl. Mater. Interfaces* **2014**, *6*, 12922 – 12930.
[110] F. W. Yuan, H. J. Yang, H. Y. Tuan, *ACS Nano* **2012**, *6*, 9932 – 9942.
[111] X. W. Gao, W. B. Luo, C. Zhong, D. Wexler, S. L. Chou, H. K. Liu, Z. C. Shi, G. H. Chen, K. Ozawa, J. Z. Wang, *Sci. Rep.* **2014**, *4*, 6095.
[112] H. Kim, Y. Son, C. Park, J. Cho, H. C. Choi, *Angew. Chem. Int. Ed.* **2013**, *52*, 5997 – 6001; *Angew. Chem.* **2013**, *125*, 6113 – 6117.
[113] J. G. Ren, Q. H. Wu, H. Tang, G. Hong, W. J. Zhang, S. T. Lee, *J. Mater. Chem. A* **2013**, *1*, 1821 – 1826.
[114] S. X. Jin, N. Li, H. Cui, C. X. Wang, *ACS Appl. Mater. Interfaces* **2014**, *6*, 19397 – 19404.
[115] C. Zhong, J. Z. Wang, X. W. Gao, D. Wexler, H. K. Liu, *J. Mater. Chem. A* **2013**, *1*, 10798 – 10804.
[116] L. Z. Ouyang, L. N. Guo, W. H. Cai, J. S. Ye, R. Z. Hu, J. W. Liu, L. C. Yang, M. Zhu, *J. Mater. Chem. A* **2014**, *2*, 11280 – 11285.
[117] C. Wang, J. Ju, Y. Q. Yang, Y. F. Tang, J. H. Lin, Z. J. Shi, R. P. S. Han, F. Q. Huang, *J. Mater. Chem. A* **2013**, *1*, 8897 – 8902.
[118] G. L. Cui, L. Gu, L. J. Zhi, N. Kaskhedikar, P. A. van Aken, K. Müllen, J. Maier, *Adv. Mater.* **2008**, *20*, 3079 – 3083.
[119] G. Cui, L. Gu, N. Kaskhedikar, P. A. van Aken, J. Maier, *Electrochim. Acta* **2010**, *55*, 985 – 988.
[120] G. Jo, I. Choi, H. Ahn, M. J. Park, *Chem. Commun.* **2012**, *48*, 3987 – 3989.
[121] J. Liu, K. P. Song, C. B. Zhu, C. C. Chen, P. A. van Aken, J. Maier, Y. Yu, *ACS Nano* **2014**, *8*, 7051 – 7059.
[122] D. T. Ngo, R. S. Kalubarme, H. T. T. Le, J. G. Fisher, C. N. Park, I. D. Kim, C. J. Park, *Adv. Funct. Mater.* **2014**, *24*, 5291 – 5298.
[123] M. X. Liu, X. M. Ma, L. H. Gan, Z. J. Xu, D. Z. Zhu, L. W. Chen, *J. Mater. Chem. A* **2014**, *2*, 17107 – 17114.
[124] G. H. Lee, S. J. Kwon, K. S. Park, J. G. Kang, J. G. Park, S. Lee, J. C. Kim, H. W. Shim, D. W. Kim, *Sci. Rep.* **2014**, *4*, 6883.
[125] X. N. Li, J. W. Liang, Z. G. Hou, Y. C. Zhu, Y. Wang, Y. T. Qian, *Chem. Commun.* **2015**, *51*, 3882 – 3885.
[126] X. Wen, X. L. Wei, L. W. Yang, P. K. Shen, *J. Mater. Chem. A* **2015**, *3*, 2090 – 2096.
[127] M. H. Seo, M. Park, K. T. Lee, K. Kim, J. Kim, J. Cho, *Energy Environ. Sci.* **2011**, *4*, 425 – 428.
[128] Y. Wang, G. X. Wang, *Chem. Asian J.* **2013**, *8*, 3142 – 3146.
[129] G. H. Yue, X. Q. Zhang, Y. C. Zhao, Q. S. Xie, X. X. Zhang, D. L. Peng, *RSC Adv.* **2014**, *4*, 21450 – 21455.
[130] P. Wu, H. Wang, Y. W. Tang, Y. M. Zhou, T. H. Lu, *ACS Appl. Mater. Interfaces* **2014**, *6*, 3546 – 3552.
[131] C. M. Hwang, J. W. Park, *Electrochim. Acta* **2011**, *56*, 6737 – 6747.
[132] X. Xin, X. F. Zhou, F. Wang, X. Y. Yao, X. X. Xu, Y. M. Zhu, Z. P. Liu, *J. Mater. Chem.* **2012**, *22*, 7724 – 7730.
[133] J. X. Cheng, J. Q. Wang, W. H. Li, X. W. Liu, Y. Yu, *RSC Adv.* **2014**, *4*, 37746 – 37751.
[134] W. Luo, X. F. Wang, C. Meyers, N. Wannenmacher, W. Sirisaksoontorn, M. M. Lerner, X. L. Ji, *Sci. Rep.* **2013**, *3*, 2222.
[135] L. P. Tan, Z. Y. Lu, H. T. Tan, J. X. Zhu, X. H. Rui, Q. Y. Yan, H. H. Hng, *J. Power Sources* **2012**, *206*, 253 – 258.
[136] L. Li, K. H. Seng, C. Q. Feng, H. K. Liu, Z. P. Guo, *J. Mater. Chem. A* **2013**, *1*, 7666 – 7672.
[137] Y. Xiao, M. H. Cao, *Chem. Asian J.* **2014**, *9*, 2859 – 2865.
[138] D. Li, C. Q. Feng, H. K. Liu, Z. P. Guo, *J. Mater. Chem. A* **2015**, *3*, 978 – 981.

[139] C. H. Yao, J. Wang, H. F. Bao, Y. F. Shi, *Mater. Lett.* **2014**, *124*, 73 – 76.
[140] X. Li, W. Guo, Q. Wan, J. M. Ma, *RSC Adv.* **2015**, *5*, 28111 – 28114.
[141] H. Y. Qiu, L. X. Zeng, T. B. Lan, X. K. Ding, M. D. Wei, *J. Mater. Chem. A* **2015**, *3*, 1619 – 1623.
[142] T. Y. Qiang, J. X. Fang, Y. X. Song, Q. Y. Ma, M. Ye, Z. Fang, B. Y. Geng, *RSC Adv.* **2015**, *5*, 17070 – 17075.
[143] W. Li, J. Zheng, T. K. Chen, T. Wang, X. J. Wang, X. G. Li, *Chem. Commun.* **2014**, *50*, 2052 – 2054.
[144] R. A. DiLeo, S. Frisco, M. J. Ganter, R. E. Rogers, R. P. Raffaelle, B. J. Landi, *J. Phys. Chem. C* **2011**, *115*, 22609 – 22614.
[145] M. W. Forney, M. J. Dzara, A. L. Doucett, M. J. Ganter, J. W. Staub, R. D. Ridgley, B. J. Landi, *J. Mater. Chem. A* **2014**, *2*, 14528 – 14535.
[146] J. Hao, N. Li, X. X. Ma, X. X. Liu, X. S. Liu, Y. Li, H. B. Xu, J. P. Zhao, *Mater. Lett.* **2015**, *144*, 50 – 53.
[147] X. H. Wang, R. A. Susantyoko, Y. Fan, L. M. Sun, Q. Z. Xiao, Q. Zhang, *Small* **2014**, *10*, 2826 – 2829.
[148] R. A. Susantyoko, X. H. Wang, L. M. Sun, K. L. Pey, E. Fitzgerald, Q. Zhang, *Carbon* **2014**, *77*, 551 – 559.
[149] J. Wang, J. Z. Wang, Z. Q. Sun, X. W. Gao, C. Zhong, S. L. Chou, H. K. Liu, *J. Mater. Chem. A* **2014**, *2*, 4613 – 4618.
[150] R. A. Dileo, M. J. Ganter, M. N. Thone, M. W. Forney, J. W. Staub, R. E. Rogers, B. J. Landi, *Nano Energy* **2013**, *2*, 268 – 275.
[151] S. L. Li, C. Chen, K. Fu, L. G. Xue, C. X. Zhao, S. Zhang, Y. Hu, L. Zhou, X. W. Zhang, *Solid State Ionics* **2014**, *254*, 17 – 26.
[152] S. L. Li, C. Chen, K. Fu, R. White, C. X. Zhao, P. D. Bradford, X. W. Zhang, *J. Power Sources* **2014**, *253*, 366 – 372.
[153] W. H. Li, Z. Z. Yang, J. X. Cheng, X. W. Zhong, L. Gu, Y. Yu, *Nanoscale* **2014**, *6*, 4532 – 4537.
[154] W. Wang, Y. Xiao, X. Wang, B. Liu, M. H. Cao, *ChemSusChem* **2014**, *7*, 2914 – 2922.
[155] S. H. Woo, S. J. Choi, J. H. Park, W. S. Yoon, S. W. Hwang, D. Whang, *J. Electrochem. Soc.* **2013**, *160*, A112 – A116.
[156] A. L. M. Reddy, M. M. Shaijumon, S. R. Gowda, P. M. Ajayan, *Nano Lett.* **2009**, *9*, 1002 – 1006.
[157] D. J. Xue, S. Xin, Y. Yan, K. C. Jiang, Y. X. Yin, Y. G. Guo, L. J. Wan, *J. Am. Chem. Soc.* **2012**, *134*, 2512 – 2515.
[158] F. W. Yuan, H. Y. Tuan, *Chem. Mater.* **2014**, *26*, 2172 – 2179.
[159] M. Nazarian-Samani, A. R. Kamali, *Powder Metall.* **2014**, *57*, 119 – 126.
[160] R. Basu, S. Bhattacharya, R. Bhatt, M. Roy, S. Ahmad, A. Singh, M. Navaneethan, Y. Hayakawa, D. K. Aswal, S. K. Gupta, *J. Mater. Chem. A* **2014**, *2*, 6922 – 6930.
[161] P. S. Chakraborty, A. S. Cardoso, B. R. Wier, A. P. Omprakash, J. D. Cressler, M. Kaynak, B. Tillack, *IEEE Electron Device Lett.* **2014**, *35*, 151 – 153.
[162] S. Stegmaier, T. F. Fässler, *Inorg. Chem.* **2013**, *52*, 2809 – 2816.
[163] V. Pavlyuk, A. Stetskiv, B. Rozdzynska-Kielbik, *Intermetallics* **2013**, *43*, 29 – 37.
[164] J. Z. Wang, N. Du, H. Zhang, J. X. Yu, D. R. Yang, *J. Mater. Chem.* **2012**, *22*, 1511 – 1515.
[165] X. Y. Zhao, C. M. Wang, D. Wang, H. Hahn, M. Fichtner, *Electrochem. Commun.* **2013**, *35*, 116 – 119.
[166] C. J. Zhang, S. P. Pang, Q. S. Kong, Z. H. Liu, H. Hu, W. Jiang, P. X. Han, D. Wang, G. L. Cui, *RSC Adv.* **2013**, *3*, 1336 – 1340.
[167] H. Tang, J. P. Tu, X. Y. Liu, Y. J. Zhang, S. Huang, W. Z. Li, X. L. Wang, C. D. Gu, *J. Mater. Chem. A* **2014**, *2*, 5834 – 5840.
[168] C. Yue, Y. J. Yu, S. B. Sun, X. He, B. B. Chen, W. Lin, B. B. Xu, M. S. Zheng, S. T. Wu, J. Li, J. Y. Kang, L. W. Lin, *Adv. Funct. Mater.* **2015**, *25*, 1386 – 1392.
[169] C. Yue, Y. J. Yu, Z. G. Wu, X. He, J. Y. Wang, J. T. Li, C. Li, S. T. Wu, J. Li, J. Y. Kang, *Nanoscale* **2014**, *6*, 1817 – 1822.
[170] M. Haro, T. Song, A. Guerrero, L. Bertoluzzi, J. Bisquert, U. Paik, G. Garcia-Belmonte, *Phys. Chem. Chem. Phys.* **2014**, *16*, 17930 – 17935.
[171] L. Romano, G. Impellizzeri, L. Bosco, F. Ruffino, M. Miritello, M. G. Grimaldi, *J. Appl. Phys.* **2012**, *111*, 113515.
[172] J. Li, C. Yue, Y. J. Yu, Y. S. Chui, J. Yin, Z. G. Wu, C. D. Wang, Y. S. Zang, W. Lin, J. T. Li, S. T. Wu, Q. H. Wu, *J. Mater. Chem. A* **2013**, *1*, 14344 – 14349.
[173] C. M. Hwang, C. H. Lim, J. W. Park, *Thin Solid Films* **2011**, *519*, 2332 – 2338.
[174] C. M. Hwang, J. W. Park, *J. Power Sources* **2011**, *196*, 6772 – 6780.
[175] Y. J. Yu, C. Yue, S. B. Sun, W. Lin, H. Su, B. B. Xu, J. T. Li, S. T. Wu, J. Li, J. Y. Kang, *ACS Appl. Mater. Interfaces* **2014**, *6*, 5884 – 5890.
[176] T. Song, H. Y. Cheng, H. Choi, J. H. Lee, H. Han, D. H. Lee, D. S. Yoo, M. S. Kwon, J. M. Choi, S. G. Doo, H. Chang, J. L. Xiao, Y. G. Huang, W. I. Park, Y. C. Chung, H. Kim, J. A. Rogers, U. Paik, *ACS Nano* **2012**, *6*, 303 – 309.
[177] T. Song, H. Y. Cheng, K. Town, H. Park, R. W. Black, S. Lee, W. I. Park, Y. G. Huang, J. A. Rogers, L. F. Nazar, U. Paik, *Adv. Funct. Mater.* **2014**, *24*, 1458 – 1464.
[178] Y. J. Cho, C. H. Kim, H. S. Im, Y. Myung, H. S. Kim, S. H. Back, Y. R. Lim, C. S. Jung, D. M. Jang, J. Park, S. H. Lim, E. H. Cha, K. Y. Bae, M. S. Song, W. Il Cho, *Phys. Chem. Chem. Phys.* **2013**, *15*, 11691 – 11695.
[179] C. L. Yan, W. Xi, W. P. Si, J. W. Deng, O. G. Schmidt, *Adv. Mater.* **2013**, *25*, 539 – 544.
[180] S. F. Fan, L. Y. Lim, Y. Y. Tay, S. S. Pramana, X. H. Rui, M. K. Samani, Q. Y. Yan, B. K. Tay, M. F. Toney, H. H. Hng, *J. Mater. Chem. A* **2013**, *1*, 14577 – 14585.
[181] M. I. Bodnarchuk, K. V. Kravchyk, F. Krumeich, S. T. Wang, M. V. Kovalenko, *ACS Nano* **2014**, *8*, 2360 – 2368.
[182] X. Pang, C. Wan, M. Wang, Z. Lin, *Angew. Chem. Int. Ed.* **2014**, *53*, 5524 – 5538; *Angew. Chem.* **2014**, *126*, 5630 – 5644.
[183] Y. Yu, C. L. Yan, L. Gu, X. Y. Lang, K. Tang, L. Zhang, Y. Hou, Z. F. Wang, M. W. Chen, O. G. Schmidt, J. Maier, *Adv. Energy Mater.* **2013**, *3*, 281 – 285.
[184] K. C. Klavetter, J. P. de Souza, A. Heller, C. B. Mullins, *J. Mater. Chem. A* **2015**, *3*, 5829 – 5834.
[185] C. H. Kim, Y. S. Jung, K. T. Lee, J. H. Ku, S. M. Oh, *Electrochim. Acta* **2009**, *54*, 4371 – 4377.
[186] J. K. Feng, M. O. Lai, L. Lu, *Electrochim. Acta* **2012**, *62*, 103 – 108.
[187] Y. J. Cho, H. S. Im, H. S. Kim, Y. Myung, S. H. Back, Y. R. Lim, C. S. Jung, D. M. Jang, J. Park, E. H. Cha, W. Il Cho, F. Shojaei, H. S. Kang, *ACS Nano* **2013**, *7*, 9075 – 9084.
[188] D. P. Lv, M. L. Gordin, R. Yi, T. Xu, J. X. Song, Y. B. Jiang, D. Choi, D. H. Wang, *Adv. Funct. Mater.* **2014**, *24*, 1059 – 1066.
[189] K. H. Seng, M. H. Park, Z. P. Guo, H. K. Liu, J. Cho, *Nano Lett.* **2013**, *13*, 1230 – 1236.
[190] Y. J. Cho, H. S. Im, Y. Myung, C. H. Kim, H. S. Kim, S. H. Back, Y. R. Lim, C. S. Jung, D. M. Jang, J. Park, E. H. Cha, S. H. Choo, M. S. Song, W. I. Cho, *Chem. Commun.* **2013**, *49*, 4661 – 4663.
[191] H. S. Im, Y. R. Lim, Y. J. Cho, J. Park, E. H. Cha, H. S. Kang, *J. Phys. Chem. C* **2014**, *118*, 21884 – 21888.
[192] P. R. Abel, K. C. Klavetter, K. Jarvis, A. Heller, C. B. Mullins, *J. Mater. Chem. A* **2014**, *2*, 19011 – 19018.
[193] S. Wu, Q. Ma, F. He, *J. Am. Ceram. Soc.* **2013**, *96*, 2046 – 2049.
[194] J. Feng, M. O. Lai, L. Lu, *Mater. Res. Bull.* **2012**, *47*, 1693 – 1696.
[195] G.-H. Lee, J.-C. Kim, D.-H. Lee, S.-D. Seo, H.-W. Shim, D.-W. Kim, *ChemElectroChem* **2014**, *1*, 673 – 678.
[196] J. K. Feng, M. O. Lai, L. Lu, *Electrochem. Commun.* **2011**, *13*, 287 – 289.
[197] R. Yi, J. Feng, D. Lv, M. L. Gordin, S. Chen, D. Choi, D. Wang, *Nano Energy* **2013**, *2*, 498 – 504.

[198] W. Chen, L. Lu, S. Maloney, Y. Yang, W. Wang, *Phys. Chem. Chem. Phys.* **2015**, *17*, 5109 – 5114.
[199] Y. Li, Y. Wang, Y. Zhang, *Sci. Adv. Mater.* **2013**, *5*, 523 – 529.
[200] F. Zou, X. Hu, L. Qie, Y. Jiang, X. Xiong, Y. Qiao, Y. Huang, *Nanoscale* **2014**, *6*, 924 – 930.
[201] F. Zou, X. Hu, Y. Sun, W. Luo, F. Xia, L. Qie, Y. Jiang, Y. Huang, *Chem. Eur. J.* **2013**, *19*, 6027 – 6033.
[202] J. Feng, C. Wang, Y. Qian, *Mater. Lett.* **2014**, *122*, 327 – 330.
[203] J. Wang, C. Q. Feng, Z. Q. Sun, S. L. Chou, H. K. Liu, J. Z. Wang, *Sci. Rep.* **2014**, *4*, 7030.
[204] S. Jin, C. Wang, *Nano Energy* **2014**, *7*, 63 – 71.
[205] W. Li, X. Wang, B. Liu, J. Xu, B. Liang, T. Luo, S. Luo, D. Chen, G. Shen, *Nanoscale* **2013**, *5*, 10291 – 10299.
[206] M.-C. Lin, M. Gong, B. Lu, Y. Wu, D.-Y. Wang, M. Guan, M. Angell, C. Chen, J. Yang, B.-J. Hwang, H. Dai, *Nature* **2015**, *520*, 324 – 328.
[207] G. Sahu, E. Rangasamy, J. C. Li, Y. Chen, K. An, N. Dudney, C. D. Liang, *J. Mater. Chem. A* **2014**, *2*, 10396 – 10403.
[208] http://cleantechnica.com/2015/05/07/high-performance-solid-state-lithium-batteries-via-thinbendable-sulfide-solid-electrolyte-films/.
[209] J. D. Ocon, J. W. Kim, S. Uhm, B. S. Mun, J. Lee, *Phys. Chem. Chem. Phys.* **2013**, *15*, 6333 – 6338.
[210] L. Baggetto, J. K. Keum, J. F. Browning, G. M. Veith, *Electrochem. Commun.* **2013**, *34*, 41 – 44.
[211] P. R. Abel, Y. M. Lin, T. de Souza, C. Y. Chou, A. Gupta, J. B. Goodenough, G. S. Hwang, A. Heller, C. B. Mullins, *J. Phys. Chem. C* **2013**, *117*, 18885 – 18890.
[212] A. Kohandehghan, K. Cui, M. Kupsta, J. Ding, E. M. Lotfabad, W. P. Kalisvaart, D. Mitlin, *Nano Lett.* **2014**, *14*, 5873 – 5882.
[213] P. R. Abel, M. G. Fields, A. Heller, C. B. Mullins, *ACS Appl. Mater. Interfaces* **2014**, *6*, 15860 – 15867.
[214] B. Farbod, K. Cui, W. P. Kalisvaart, M. Kupsta, B. Zahiri, A. Kohandehghan, E. M. Lotfabad, Z. Li, E. J. Luber, D. Mitlin, *ACS Nano* **2014**, *8*, 4415 – 4429.
[215] C. Li, S. Jiang, J. W. Lv, T. Zheng, *J. Alloys Compd.* **2015**, *633*, 246 – 249.
[216] C. Masquelier, *Nat. Mater.* **2011**, *10*, 649 – 650.
[217] T. Hakari, M. Nagao, A. Hayashi, M. Tatsumisago, *J. Power Sources* **2015**, *293*, 721 – 725.
[218] C. R. Mariappan, M. Gellert, C. Yada, F. Rosciano, B. Roling, *Electrochem. Commun.* **2012**, *14*, 25 – 28.
[219] K. Arbi, W. Bucheli, R. Jimenez, J. Sanz, *J. Eur. Ceram. Soc.* **2015**, *35*, 1477 – 1484.
[220] H. S. Jadhav, R. S. Kalubarme, S. Y. Jang, K. N. Jung, K. H. Shin, C. J. Park, *Dalton Trans.* **2014**, *43*, 11723 – 11727.
[221] Y. J. Liu, B. J. Li, H. Kitaura, X. P. Zhang, M. Han, P. He, H. S. Zhou, *Acs Appl. Mater. Interfaces* **2015**, *7*, 17307 – 17310.
[222] H. Kitaura, H. Zhou, *Sci. Rep.* **2015**, *5*, 13271.
[223] Y. C. Jung, S. M. Lee, J. H. Choi, S. S. Jang, D. W. Kim, *J. Electrochem. Soc.* **2015**, *162*, A704 – A710.
[224] Y. Hirobe, Tdk Corp (Denk-C), S. 13.
[225] N. Kamaya, K. Homma, Y. Yamakawa, M. Hirayama, R. Kanno, M. Yonemura, T. Kamiyama, Y. Kato, S. Hama, K. Kawamoto, A. Mitsui, *Nat. Mater.* **2011**, *10*, 682 – 686.
[226] S. P. Ong, Y. F. Mo, W. D. Richards, L. Miara, H. S. Lee, G. Ceder, *Energy Environ. Sci.* **2013**, *6*, 148 – 156.
[227] J. Y. Yin, X. Y. Yao, G. Peng, J. Yang, Z. Huang, D. Liu, Y. C. Tao, X. X. Xu, *Solid State Ionics* **2015**, *274*, 8 – 11.
[228] J. D. Ocon, J. W. Kim, S. Uhm, B. S. Mun, J. Lee, *Phys. Chem. Chem. Phys.* **2013**, *15*, 6333 – 6338.
[229] O. I. Malyi, T. L. Tan, S. Manzhos, *J. Power Sources* **2013**, *233*, 341 – 345.

Received: October 14, 2015
Published online: June 9, 2016

